Study of a Hydrodynamic Thrust Bearing for Hydroelectric Power Stations

Francisco Morais Magalhães Marques de Sousa

U.PORTO

FEUP FACULDADE DE ENGENHARIA
UNIVERSIDADE DO PORTO

Study of a Hydrodynamic Thrust Bearing for Hydroelectric Power Stations

Francisco Morais Magalhães Marques de Sousa

Master thesis presented to
Faculdade de Engenharia da Universidade do Porto

Thesis supervised by
Prof. Ramiro Carneiro Martins
Eng. Filipe Duarte

Porto, September of 2016

Acknowledgements

To my supervisor in EDP, Eng. Filipe Duarte, for all his guidance and patience, the experience transmitted and for always finding time to help me, my sincere gratitude for his teachings. Also, I would like to express my gratitude to Eng. Alexandre Ferreira da Silva for his support and guidance throughout this work, and for his incentive to always prime for scientific rigour. Finally, to all the remarkable people I shared the office with in this company, I would like to thank for receiving me so kindly and all the support given.

To my supervisor in FEUP, Prof. Ramiro Martins, for all his guidance and patience and all the support given through this work. To my colleagues and friends from my college for their support and encouragement.

I would like to thank and dedicate this thesis to my family for their constant presence and unconditional support and for all their effort so that I always had everything I needed. Finally, to my childhood friends and my team mates, a word of appreciation for all their motivation and encouragement.

Abstract

For over a century, hydrodynamic thrust bearings have been used to support the weight and the hydraulic load of hydro generators. Born from the experiments of Tower and the theoretical work of Reynolds, these fluid film bearings can support hundreds of tons of load on a thin oil film and work for decades with negligible wear.

The objective of this work is to analyse a thrust bearing by calculating the pressure distribution of the oil film between the pad and the runner and the load capacity.

Firstly, an analytical solution based on the Reynolds theory of lubrication to the hydrodynamic pressure distribution along the pad will be presented, considering a simplified geometry of the pad and the flow to be isoviscous and isothermal. Secondly, the Reynolds equation will be written in a finite difference equation through a truncated Taylor series expansion and implemented in a Finite Differences Method algorithm. The solution will produce the pressure distribution over the pad and the optimum minimum film thickness and tilting.

Sumário

Há mais de um século que chumaceiras hidrodinâmicas de impulso são utilizadas para suportar o peso e carga hidraulica de turbinas em geradores hidroelétricos. Criadas a partir do trabalho experimental de Tower e do trabalho teórico de Reynolds, estas chumaceiras podem suportar centenas de toneladas de carga num filme de óleo e trabalhar décadas sem causar desgaste substancial.

O objectivo deste trabalho é analisar uma chumaceira de impulso através do cálculo da distribuição de pressões no filme de óleo entre o patim e o espelho e a capacidade de carga gerada.

Primeiramente será apresentada uma solução analítica uni-dimensional baseada na teoria de lubrificação de Reynolds para a distribuição de pressão ao longo do patim. considerando um patim de dimensões simplificadas e um escoamento de óleo isoviscoso e isotérmico. Em segundo lugar, a equação de Reynolds será escrita como um equação de diferenças finitas através de uma expansão em série de Taylor e implementada num código de método das diferenças finitas. A solução irá fornecer a distribuição de pressão sobre o patim e os valores óptimos para a espessura mínima de filme e para a inclinação do patim.

Contents

Acknowledgements v
Abstract vii
Sumário viii
Table of contents ix
Table of Figures xi
List of Tables xiii

1. Introduction **1**
1.1. Objectives 2
1.2. Document Structure 2

2. Hydrodynamic Thrust Bearings for Hydroelectric Plants **5**
2.1. Historical Background 5
2.2. Introduction 6
2.3. Mechanism of Pressure Development in Fluid Film Lubrication 8
2.4. Thrust Bearing Design 9
2.4.1. Lubrication 12
2.4.2. Operational Limits and Temperature Monitoring 13
2.4.3. Auxiliary Systems 15

3. Thrust Bearing Geometry and Operating Conditions **19**
3.1. Introduction 19
3.2. Operating Conditions 19
3.3. Thrust Bearing Pad Geometry 20
3.3.1. Pad surface 21

4. Hydro Generator Start-Up Procedure: Hydrostatic Lifting **25**
4.1. Introduction 25
4.2. Hydro Generator Start-up 25
4.2.1. Analysis of the Lifting Procedure 26
4.3. Conclusions 27

5. Analytical Solution for Pressure Distribution in Hydrodynamic Lubrication **29**
5.1. Introduction 29
5.2. Reynolds Equation 29
5.3. Thrust Bearing Fixed-Inclined Pad Geometry 31
5.3.1. Ramp Analysis 32
5.4. Hydrodynamic Pressure Distribution 34
5.4.1. Results 36
5.5. Conclusions 37

6. Numerical Solution for Pressure Distribution in Hydrodynamic Lubrication **39**
6.1. Introduction 39
6.2. Numerical Methods 39
6.2.1. Finite Difference Method 40
6.3. Reynolds Equation 42
6.4. Computational Procedure 43
6.5. Results 44
6.5.1. Fixed-Inclined Pad 44
6.5.2. Optimum Minimum Film Thickness and Tilting 45
6.6. Conclusions 46

7. Conclusions and Future Work Perspectives **49**
7.1. Future Work 49

Bibliography **51**

Appendices **53**

A. MATLAB Code **55**

List of Figures

2.1. Kinsgbury's first hydrodynamic thrust bearing [1] 6
2.2. A sketch by Albert Kingsbury [1] 6
2.3. Combined Hydrodynamic bearing in a large hydro generator unit [2] . 6
2.4. Francis Turbine 7
2.5. Couette flow [3] 8
2.6. Poiseuille flow [3] 8
2.7. Resulting velocity profile in a flow between two non-parallel plates [3] 8
2.8. Thrust bearing part schematic [4] 10
2.9. Misalignment, edge load and equalizing schematic for (a) tapered land and line contact pivots, (b) spherical pivoted shoes, and (c) equalizing feature. [5] 11
2.10. Hydrodynamic thrust bearing for a reversible hydro generator [2] . . . 11
2.11. Stribeck Curve [6] 13
2.12. Limits of safe operation for tilting pad bearings [7] 14
2.13. Temperature measurement points in a thrust pad as suggested by Leopard and Garner in [8] 15
2.14. Representation of thermocouple mounting as suggested by Glavatskih [9] 16
2.15. Vertical Thrust Bearing Oil Sump and Cooling Coils [4] 17

3.1. Example of a thrust bearing pad 20
3.2. Detail of the recess 21
3.3. Thrust bearing pad design 22
3.4. Detail of the surface of the pad represented with inflated convexity . 22
3.5. Example of the type of contact between the pad and the runner [10] . 23
3.6. Example of a pressure distribution inside a linear contact [10] 23

5.1. Thrust bearing geometry [3] 31
5.2. Thrust Pad and Runner Simplified Geometry 32
5.3. Scheme of the ramp and runner. [3] 33
5.4. Pressure distribution of fixed-inclined slider bearing [3] 35
5.5. Analytical solution for the pressure distribution 37

6.1. FDM approximation using two adjacent nodes [11] 40
6.2. Nodal scheme for numerical analysis of the Reynolds equation [11]. . 41
6.3. Discretization of the pad with 36x36 nodes 42
6.4. Film height over the pad 45
6.5. Pressure distribution in the oil film 46
6.6. Film height over the pad 46
6.7. Pressure distribution in the oil film 47
6.8. Pressure distribution in the oil film 47

List of Tables

3.1. Bearing operating conditions and oil properties 19
3.2. Bearing Geometry 20
3.3. Data for the Hertz contact theory calculations 23

4.1. Hydrostatic lift parameters 26

5.1. Ramp geometry and operating conditions 33
5.2. Pad geometry 34

List of Symbols

a	half-width of the contact area, m
b	Pad width, m
E	Young modulus, GPa
E^*	Equivalent Young modulus, GPa
F_n	Normal load, N
h	Oil film thickness, μm
h_0	Minimum oil film thickness, μm
h_m	Oil film thickness when the pressure gradient is equal to zero, μm
H_0	Dimensionless minimum oil film thickness, $H_0 = \frac{h_0}{s_h}$
L	Length of the pad, m
L_1	Length of the ramp of the pad, m
L_2	Length of the horizontal part of the pad, m
N_p	Number of pads
p	Pressure, Pa
P_{mx}	Maximum pressure, Pa
r	Radius, m
r_i	Bearing inside radius, m
r_o	Bearing outside radius, m
Re	Reynolds Number
R_x	Equivalent radius in the x coordinate, m
R_{x_1}	Radius of the surface pad in the x coordinate, m
R_{x_2}	Radius of the surface runner in the x coordinate, m
s_h	Difference between the maximum and the minimum oil film thickness, μm
U	Average linear speed, $m \cdot s^{-1}$
w'	Normal load capacity per unit width, $N \cdot m^{-1}$
W	Normal load capacity per pad, N
W_{total}	Normal load capacity of the bearing, N
X	Dimensionless x coordinate, $X = \frac{x}{L}$
β	Angular extent of the pad, rad
μ	Dynamic viscosity, $Pa \cdot s$
ν	Kinematic viscosity, cSt
ω	Angular speed, $rad \cdot s^{-1}$
ρ	Density, $kg \cdot m^{-3}$
θ	Angle, rad

1. Introduction

In a modern era where renewable energies play a core role in the energy production business, hydroelectric power is the second biggest source of energy in Portugal, representing almost 8 % of the total electric energy distributed by EDP - Energias de Portugal, S.A. in 2015 to household and small businesses.

Despite having a significantly smaller contribution than wind power, which achieved approximately 53 % of the total electric energy distributed in 2015, the several facilities with high water storage capacity possess a big advantage: dispatchable generation. This term is used to describe a source that, whenever there is a deficit in the electrical grid, can be activated by an operator and start generating energy within a small amount of time. In the case of hydroelectric plants, it is only a matter of seconds between giving the order and having a full power production regime. Since it is impossible to predict accurately the output of wind power generation, hydropower is the answer to maintain a stable power grid.

The most recent type of hydroelectric plant is the pumped storage. The type of construction is the same as an impoundment - it has a big reservoir - but instead of turbines the machines can work both as a turbine and a pump, sending the water upstream when needed. This recent concept allows these facilities to work as a battery. When there is more production of energy than demand, for example from sources from which it is not possible to control the output, this excess of energy is used to pump water upstream so it can be used later in hours when there is a bigger demand.

In the area of hydroelectric power production, the mechanical equipment has rather unusual dimensions. All the components involved are much bigger, with shafts that can have as much as one metre of diameter or more and hydraulic circuits and valves with flow rates that reach hundreds of cubic metres per second. Therefore, each plant has unique components that were designed and built specifically for those conditions. As a consequence of the size of the machine's components, the difficult access to the plants, as most of them are in remote places, and difficult conditions and high costs for maintenance, the most important characteristic associated with these projects, besides safety, is reliability.

In a relatively recent area as Tribology, that has had its biggest development during the last century, manufacturing bearings that support hundreds of tons and run several decades without any maintenance, has been one of the biggest challenges in these projects. However, the state of art on hydrodynamic thrust bearings for turbines allow these first ones to run for many decades without any substantial wear in any of the components, even despite their frequent stop and start cycles.

1.1. Objectives

The main objective of this thesis is the analysis of a hydrodynamic thrust bearing installed in the hydroelectric plant of Frades II, situated in the north of Portugal. This plant is not active yet as its construction was concluded recently. The lubricant flow inside this bearing will be analysed, its pressure distribution and load capacity will be calculated through both analytical and numerical methods.

An analytical solution will be presented through the hydrodynamic lubrication theory of Osborne Reynolds. Several simplifications are introduced in order to allow solving the equation. The flow will be considered isoviscous and isothermal and the pressure distribution will be one dimensional, in the circumferential direction.

Regarding the numerical solution for the pressure distribution, the Finite Differences Method will be applied. The Reynolds equation will be rewritten under algebraic form through a Taylor series expansion. The radial direction, also known as "side leakage", will now be considered, thus the pressure field will be bi-dimensional.

1.2. Document Structure

2. Hydrodynamic Thrust Bearings for Hydroelectric Plants

The second chapter will be dedicated to the design and state of art of hydrodynamic thrust bearings for hydroelectric plants. First, an historical background of these bearings is presented. Secondly, the mechanism of pressure development in the fluid is explained. In the third place the design of components will be described, including their operational limits, lubricant selection and lubrication regime and power losses. Last of all, the auxiliary systems present in these bearings will be mentioned.

3. Thrust Bearing Geometry and Operating Conditions

In the third chapter the geometry and operating conditions of the thrust bearing that is object of study are presented.

4. Hydro Generator Start-Up Procedure: Hydrostatic Lifting

The third chapter will be focused on the start up procedure of the hydro generator. This chapter includes several examples of different hydro generators in other hydroelectric plants, with different pad designs and a substantial range of weight of the machine. The oil injection system for the hydrostatic lift of the rotating parts is described as well as its operation.

5. Analytical Solution for Pressure Distribution in Hydrodynamic Lubrication

In this chapter a one dimensional pressure distribution on the oil film along the circumferential direction will be presented through the hydrodynamic lubrication theory

of Osborne Reynolds. A fixed-inclined pad with a simplified geometry will be considered. Furthermore, the load-carrying capacity will also be calculated based on the pressure distribution obtained.

6. Numerical Solution for Pressure Distribution in Hydrodynamic Lubrication

The fifth chapter will be dedicate to a numerical analysis of the pressure distribution on the pad. The Reynolds equation will be transformed in a algebraic equation though a Taylor series truncated expansion. This finite difference equation will be then implemented in a FDM algorithm that uses three consecutive nodes for the approximations to the derivatives. Finally, the optimum values for minimum film thickness and tilting in a inclined pad will be presented.

7. Conclusions

In the last chapter, the general conclusions of this work and suggestions for future work will be presented.

2. Hydrodynamic Thrust Bearings for Hydroelectric Plants

2.1. Historical Background

Fluid film bearings were invented in the end of the 19^{th} century. Beauchamp Tower and Osborne Reynolds were the pioneers in research and development of these machine elements. Tower (1880) experimented and demonstrated for the first time the existence of a pressure wave in a hydrodynamic journal bearing. A few years later, Reynolds (1886) derived the classical theory of hydrodynamic lubrication. A large volume of analytical and experimental research work in hydrodynamic lubrication has subsequently followed the work of Reynolds. The classical theory of Reynolds is based on several assumptions that were adopted to simplify the mathematical derivations, most of which are still applied today. Most of these are justified because they do not result in a significant deviation from the actual conditions in the bearing. However, some other classical assumptions are not realistic but were necessary to simplify the analysis. The hydrodynamic theory of lubrication solves for fluid velocity, pressure distribution and load capacity. As in other disciplines, the introduction of computers permitted complex hydrodynamic lubrication problems to be solved by numerical analysis and have resulted in the numerical solution of such problems under realistic conditions without having to rely on certain inaccurate assumptions [12].

The first hydrodynamic thrust bearing with pivoted pads to be used in a hydroelectric plant, Figure 2.1, was invented by Albert Kingsbury and it was installed in 1912 in Holtwood, Pennsylvania in a 12 MW turbine. Back then, roller bearings were being used to support the turbines, but they were causing extensive down times, and this problem led to the search of new solutions. This first hydrodynamic bearing, after working for 75 years with negligible wear under a load of 220 tons, was considered, by ASME, the 23rd International Historic Mechanical Engineering Landmark in 1987 [1].

"The maximum pressure would occur somewhat beyond the center of the bearing block in the direction of motion and the resultant would be between that maximum and the center line of the block. It occurred to me that if the block were supported from below on a pivot, at about the theoretical center of pressure, the oil pressures would automatically take the theoretical form, with a resulting small bearing friction and absence of wear of the metal parts, and that in this way a thrust bearing could be made, with several such blocks set around in a circle and with proper arrangements for lubrication." - Albert Kingsbury [1]. The sketch which was next to this text in the note of Kingsbury is shown in Figure 2.2.

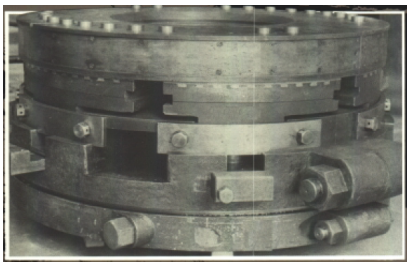

Figure 2.1.: Kinsgbury's first hydrodynamic thrust bearing [1]

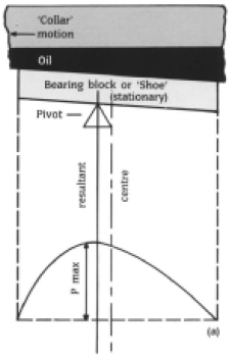

Figure 2.2.: A sketch by Albert Kingsbury [1]

2.2. Introduction

Hydrodynamic thrust bearings hold the axial position of rotating shafts, transmitting the load to the stationary casing by means of a thin film of lubricant. The bearings are used in a wide variety of rotating machinery including turbines, compressors, pumps, motors, generators, gear boxes, and many custom applications. Bearing sizes range from 5.2 m in diameter, which can carry loads on the order of 50 million newtons, down to 50 mm and smaller diameter bearings that support rotors spinning tens of thousands of revolutions per minute [5].

The function of thrust bearings in hydroelectric plants, as mentioned, is to support the hydro generator, which includes its weight and the hydraulic load. Figure 2.3 represents a combined bearing, a thrust and a journal bearings that share the same

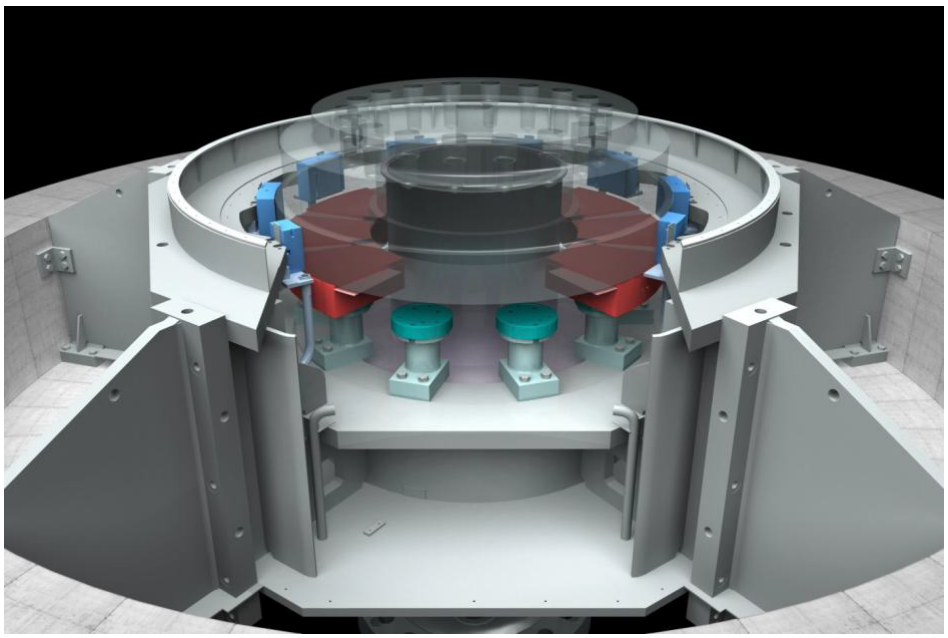

Figure 2.3.: Combined Hydrodynamic bearing in a large hydro generator unit [2]

runner, in a large hydro generator. The runner is represented in a semitransparent shape, the thrust bearing pads in red and the journal bearing pads in a darker blue. There are two possible positions for the thrust bearing: between the turbine and the alternator or above the alternator. Although both of them are common, the first solution provides a more compact arrangement, taking advantage of the rigidity of the head cover. This is exemplified in Figure 2.4, where the thrust bearing, marked with the number 1, transmits the vertical load to a steel structure with a conic shape that is represented in grey line, which, in turn, transmits the load to the head cover that is supported by the concrete structure that houses the spiral case.

Marked with number 2, there is a journal bearing. These are responsible for keeping the shafts aligned and absorbing radial loads. While there is only one thrust bearing per machine, there have to be at least two journal bearings. The reason for having only one of the first type is the impossibility of having enough precision in stack-up of tolerances and in the assembly of the components on the order of the oil film thickness in the bearing, which is generally between 25 and 100 μm. Regarding journal bearings, only one can not block rotations of the shaft in a vertical plane.

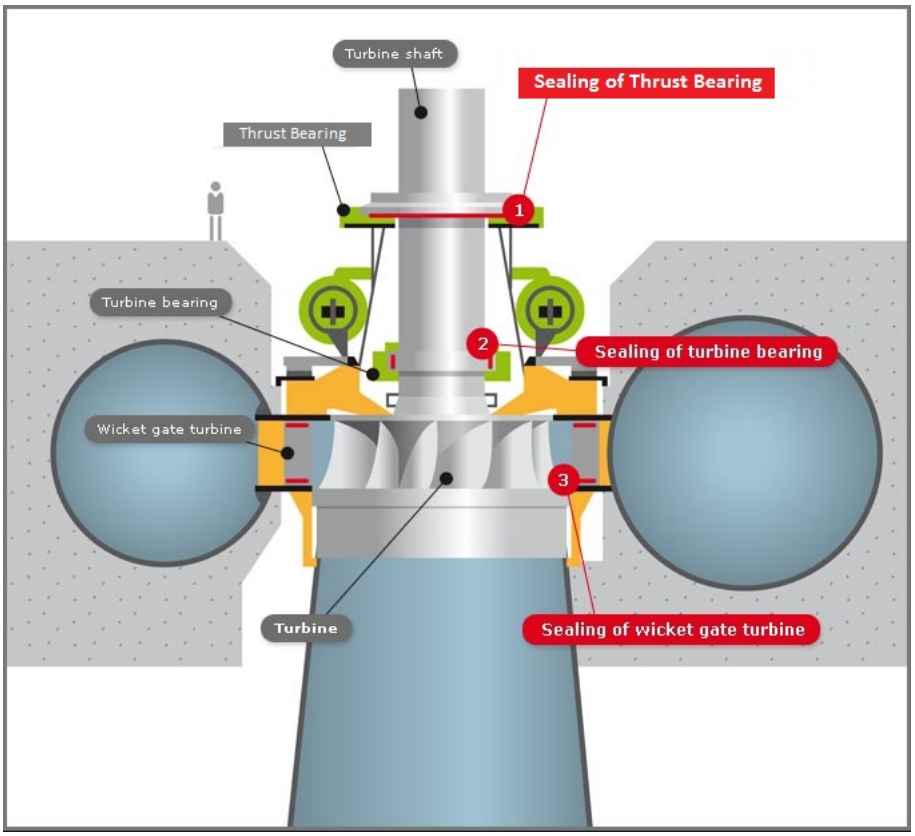

Figure 2.4.: Francis Turbine

2.3. Mechanism of Pressure Development in Fluid Film Lubrication

Hydrodynamic lubrication is the fluid dynamic effect that generates a fluid film that completely separates two surfaces in relative motion. This effect causes a hydrodynamic pressure wave in the fluid film that generates load carrying capacity. This pressure build up is a result of the lubricant being drawn into a clearance between two converging surfaces [12].

This phenomenon can be better understood by analysing the pressure development mechanism. Two non-parallel plates are shown in Figure 2.7. These are considered

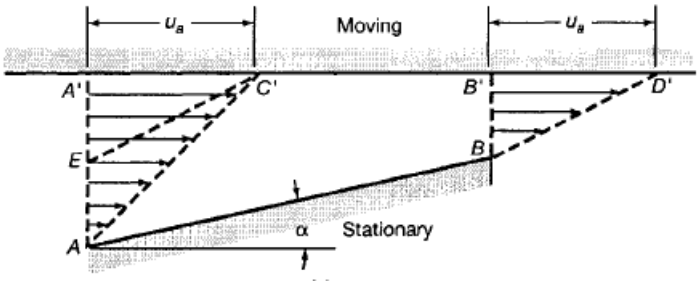

Figure 2.5.: Couette flow [3]

Figure 2.6.: Poiseuille flow [3]

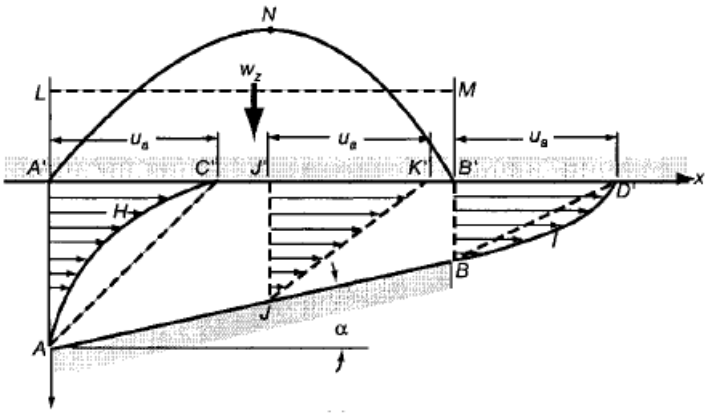

Figure 2.7.: Resulting velocity profile in a flow between two non-parallel plates [3]

to be infinitely wide, so no flow is to be considered in the direction perpendicular to the paper. The upper plate is moving with velocity u_a and the lower one is stationary. The volume of fluid that tends to be carried into the space between the surfaces through section $A'A$ is $AA'C'$. The volume of fluid that tends to be dragged out from between the surfaces through $B'B$ is $BB'D'$. Since section $A'A$ is bigger than $B'B$, volume $AA'C'$ is bigger than volume $BB'D'$. However, from flow continuity, it is known that the volume per time unit that enters AA' has to be exactly the same as the one that exits through BB' [3].

In summary, there will be a pressure build up as the section decreases that will equalize the flow rates in and out of the control volume. Figure 2.6 illustrates the velocity profiles due to Poiseuille flow. This flow is outward from both edges since flow is always from a region of higher pressure to a lower pressure one. This flow has the same direction as Couette flow on the trailing edge but an opposite direction on the leading edge [3].

The result is a combination of Couette and Poiseuille flows, as it is shown in Figure 2.7. The form of the velocity distribution in this flow satisfies the condition of equal flow rate through sections AA' and BB'. The middle profile, where the velocity gradient is constant, is where the pressure gradient is equal to zero and, thus, the pressure reaches its maximum value [3].

2.4. Thrust Bearing Design

The hydrodynamic load capacity is proportional to the sliding speed and the fluid viscosity. Similarly, the load capacity increases substantially with the decreasing of the film height. However, there is a limit and a minimum film thickness must be imposed by bearing designers. Very thin films are highly undesirable specially in machines with higher levels of vibrations. Also, there is always the risk of contact between surfaces that causes severe wear. Therefore, a crucial stage of these projects is choosing the optimum film thickness [12].

The main components of a thrust bearing are represented in Figure 2.8. The runner is a metallic disc that can be attached to the shaft by a key and nut or shrink fit, or be an integral part of it. There are two essential characteristics of the runner [4]:

- The stack-up of tolerances and misalignment has to be less than the oil film thickness, or some means of adjustment has to be incorporated;
- The surface must be flat and smooth in comparison to the film thickness, but not so smooth as to substantially diminish the adhesion of the lubricant to the surface.

The pad is usually referred as an assembly for being composed by three features [4]:

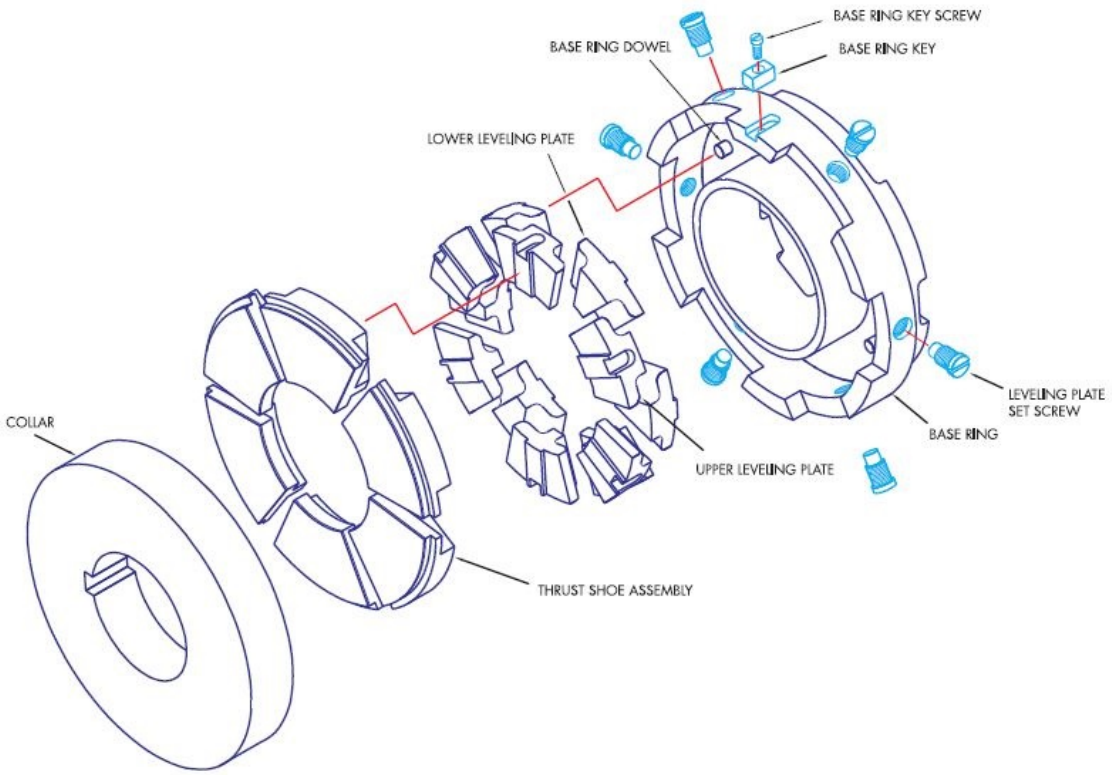

Figure 2.8.: Thrust bearing part schematic [4]

1. **Babbitt** - It is layer of a high tin alloy metallurgically bonded to the body. This is a soft material when compared to the runner and has a low friction coefficient. Its main function is to assure minimal damage on the generator in case there is a disruption of the oil film and the pad and the runner come in contact, providing enough time for an operator to stop the machine in safety. The babbitt also traps and embeds contaminants, avoiding these particles to damage other surfaces.

2. **Body** - The body is the supporting structure where the babbitt layer is deposited and allows freedom to pivot. The material is typically steel.

3. **Pivot** - Allows the pad to tilt and provide better conditions for the formation of the oil film.

The support of the pads is composed by two distinct components: the base ring and the equalizing system. Figure 2.9 illustrates the differences between three different solutions for thrust bearings alignment design. Besides the main function of load transfer from the pads to the foundation, these also equalize the load in each pad. There are different designs to assure better load distribution:

· without any load equalizing;
· Plate Spring;
· Spring Mattress;

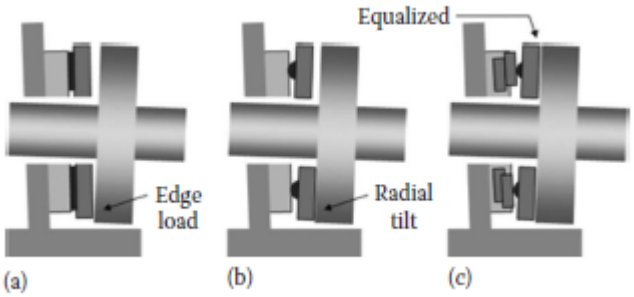

Figure 2.9.: Misalignment, edge load and equalizing schematic for (a) tapered land and line contact pivots, (b) spherical pivoted shoes, and (c) equalizing feature. [5]

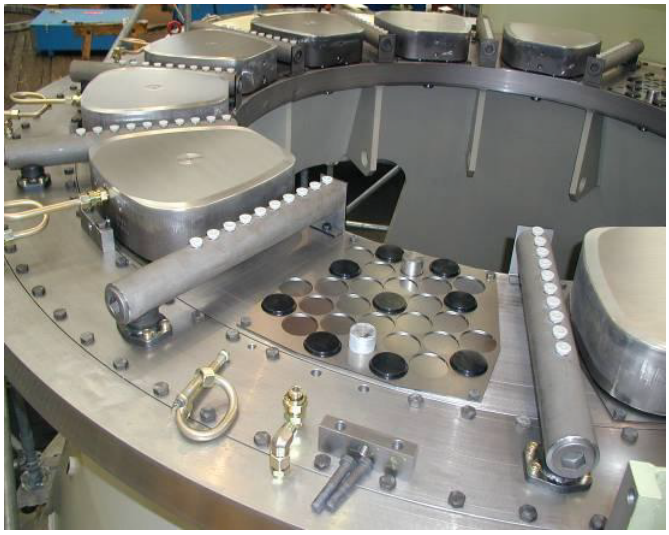

Figure 2.10.: Hydrodynamic thrust bearing for a reversible hydro generator [2]

· Hydraulic equalizing.

For large thrust bearings that support reversible machines, a common solution for the equalizing system is shown in Figure 2.10. The rubber spring mattress has a symmetrical distribution for both side tilting and the two metallic cylinders that protrude from the mattress are the pivots where the pad will be assembled. The base ring is the steel structure that supports the spring mattresses and transmits the load to the foundation. It is also possible to observe the oil injectors between the pads that will inject cold oil into the contact.

It is important to assure that pads are free to tilt in both directions. The tangential tilting is important due to the inclination of the pad and the hydrodynamic pressure generation. Radial tilting compensates thermal and elastic deformations of the components. Pad and runner sliding surfaces remain almost parallel in the radial direction, for this reason, in the hydro generators, almost all the pads are supported by point contact [2].

According to [13], where alignment inaccuracies in a large trust bearing and its consequences were studied, the bad distribution of load led to the rise of temperature in the overloaded pads and a decrease of the oil film thickness. In other words, assuring a correct load distribution, even despite some alignment inaccuracies, is essential to guarantee good conditions for the bearing to operate, avoiding excessive temperatures and loads that might damage the layer of anti friction metal.

2.4.1. Lubrication

Oil Selection

In hydroelectric plants, it is essential to pay attention to the handling of water polluting substances, like oils. These are used to lubricate bearings, auxiliary machinery and hydraulic functions in control and governing equipment. When selecting the lubricants, operating conditions of the hydroelectric plants have to be considered. The oils must display good water and air release, low foaming, good corrosion protection, good ageing resistance and compatibility with standard elastomers. Since there are no established standards for hydro generators oils, the existing product specifications for general turbine oils are adopted as basic requirements. [14]

The viscosity of these oils depends on the type and design of the turbine as well as its operating temperatures. Although the viscosity of these oils can range from 46 to 460 cSt at 40 ^oC, in many cases the selected viscosity is between 68 and 100 cSt. Water turbine oils are subject to little thermal stress, and as oil tank volumes tend to be high, the life of these lubricants is very long. [14].

Lubrication Regime

Figure 2.11 is a representation of the Stribeck curve. Hydrodynamic bearings, as the name suggests, work on "Regime I: Hydrodynamic Lubrication", the region of the graphic on the right. Since the main priorities for this application are reliability and durability, it is important to assure the two surfaces, runner and pad, will never come in contact, even in transient states where loads can reach considerably higher values. Particularly due to the characteristics of the babbitt metal that covers the pad surface, that can be damaged very easily in case of contact with the runner during machine operation and loose the capacity to perform its functions.

Regarding the efficiency of the hydrodynamic bearings, the lubrication regime is not the ideal. The Stribeck curve reaches a minimum value for the friction coefficient in the region of mixed-film lubrication, where, as exemplified in the small drawings above the curve, there is contact between surfaces. With the development of numerical methods that allow a more accurate knowledge of the film height and pressure and temperature distribution over the pad, the sizing of these bearings has become more precise, not being necessary to work with such high values of safety coefficients.

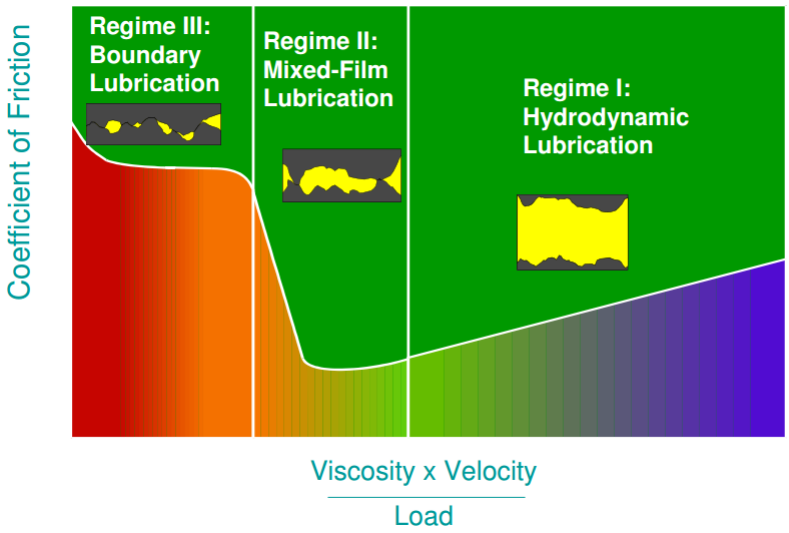

Figure 2.11.: Stribeck Curve [6]

Therefore, there has been a tendency to push the lubrication regime to the left in order to diminish the coefficient of friction and thus lower the power loss values. Nevertheless, it is forbidden to allow contact between surfaces, it is therefore imperative that lubrication is always hydrodynamic. The increase of efficiency by decreasing losses between surfaces with relative movement is one of the main matters studied in area of Tribology, which has allowed the increasing of machine performance since its beginning [15].

2.4.2. Operational Limits and Temperature Monitoring

Operational Limits

Although a more conservative approach is always advised when sizing these machine elements, over time, the tendency has been to push the bearings to their operational limits, thus increasing both the efficiency and the reliability of the bearings [2]. Over the past years, with the development of numerical methods and software that allow more accurate analysis, there is a better perception of the characteristics of the flow. By achieving a better understanding of the evolution of pressure and temperature fields between surfaces, it possible to adapt the design and optimize the geometry of the bearing and other parameters as the type of lubricant and the temperature at which it is supplied to the bearing.

A. J. Leopard, in [7], exposes the operation limits of tilting pad bearings. Firstly, the hydrodynamic limit: the bearing must operate according to hydrodynamic principles, therefore, conditions for the establishment and constant presence of a fluid film between surfaces with a minimum thickness must be guaranteed. Secondly, design and environmental limits. For a tilting pad bearing operating under certain lubrication conditions, limits can be established for safe operation in a graphic of load versus

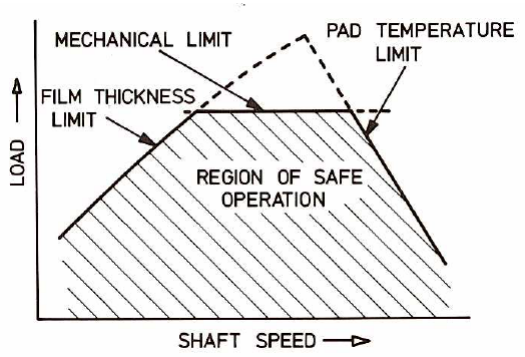

Figure 2.12.: Limits of safe operation for tilting pad bearings [7]

sliding speed, as can be seen in Figure 2.12.

For high speed rotation, the temperature on the pad surface is the dominant factor. In fact, tin based alloys, despite having a melting temperature of 239 ^oC, start to weaken at much lower temperatures. It has been determined that deformation of the babbitt layer is likely to occur for temperatures higher than 160 ^oC. Therefore, this is usually considered the absolute limit at which bearings can operate without permanent damage. However, for design purposes, it is rare to allow more than 130 ^oC for continuous operation [7].

Temperature Monitoring

Temperature monitoring in fluid film bearings is a preventive procedure that is essential to detect overheat and prevent damage to the bearing. Although it is relatively simple to measure temperature in the bearings, unless the proper locations are monitored, the results can be deceiving as to what is really happening, thus providing poor information on the overall performance of the bearing [9].

Temperature is the only parameter which can be measured to monitor the conditions within a bearing. Despite being possible to measure also the oil film thickness and the pressure distribution on the oil film, these are very difficult to measure and the results are difficult to interpret. As to measuring the levels of vibration by recording the shaft relative displacement, the results can be easily masked by external machine and foundation influences. Traditionally, the temperature of the oil that just left the bearing used to be recorded. However, this is also not a good parameter since it can have poor sensitivity and response to changing conditions within the oil film. [8]

The most common type of sensors used are thermocouples and resistance temperature detectors (RTD). From a bearing designer point a view, the thermocouples are preferred rather than RTDs [8]. Thermocouples are small, inexpensive and have rapid response time [9]. RTDs have a minimum diameter which may not fit some bearing pads and some of them are not tip sensitive. For example, the sensing element may measure the average temperature over a significant length, while all the

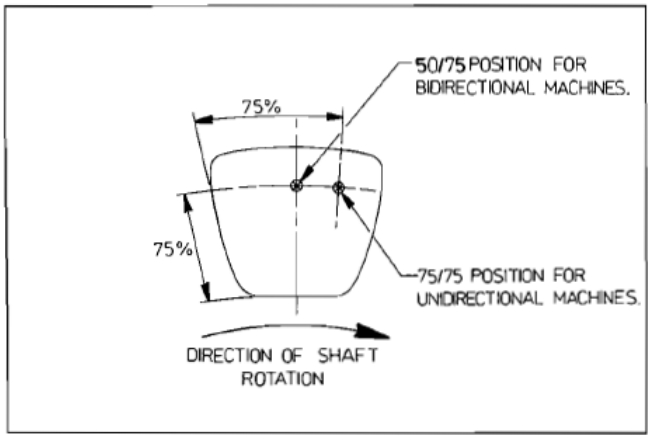

Figure 2.13.: Temperature measurement points in a thrust pad as suggested by Leopard and Garner in [8]

thermocouples are tip sensitive, by nature [8].

One of the traditional methods for installing the sensors are to bond these in the backing material near to the surface or even in the babbitt layer. Figure 2.13 represents a suggestion of where to place the sensors in the pads according to Leopard and Garner [8]. As was mentioned before, misalignment and machining tolerances cause significant differences in individual pads. Therefore it is good practice to place sensors in at least two pads, approximately 180^o apart [8].

In a more recent article, Glavatskih [9] proposes a different method for temperature monitoring. Figure 2.14 illustrates the way this author placed the thermocouples in a industrial bearing. The objective was to provide oil circulation around the thermocouple tip. The tapping holes on the anti-friction layer must be made small to minimise the effect on hydrodynamic pressure.

Relatively to the method used by Leopard and Garner [8], Glavatskih [9] chose different positions for the sensors. Moreover, several sensors were placed per pad in order to obtain a better temperature distribution on the oil film. One of the conclusions drawn on bearings coated with PTFE (Polytetrafluoroethylene) is, due to the good thermal insulation properties of this polymer, if the sensor is measuring the temperature under the PTFE layer and there is no contact with the oil, the temperature recorded will be far from the real one in the oil film. As to the babbitt, the thermal insulation is not so good, therefore this effect is not so relevant.

2.4.3. Auxiliary Systems

The housing of the bearing has an additional function of oil tank, since the bearing is usually immersed in oil. Figure 2.15 shows the housing of a vertical thrust bearing. Three different areas can be distinguished:

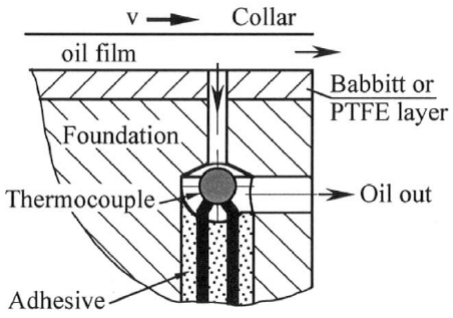

Figure 2.14.: Representation of thermocouple mounting as suggested by Glavatskih [9]

- The inner part where the pads are, in which there is an injection system that supplies oil from the main oil tank;
- The outer part, where there is a cooling system composed by coils that will be in the middle of warm oil that just left the bearing;
- Above these last two will be an air chamber, to accommodate thermal expansions of the oil.

A cooling system is required to remove the heat generated by oil shear before re-entering the bearing [4]. The cooling system represented in Figure 2.15 is internal. This solution has several disadvantages such as oil contamination in case of water leak in the coils that are inside the tank, which would demand the disassembly of the bearing for repair. The temperature variation of the water with the seasons of the year also implies a loss in efficiency, since the flow of these cooling systems is usually non adjustable. For asynchronous generators, where the rotating speed is variable, the convection coefficient between the oil and the coils will also vary, thus diminishing efficiency. [2].

The most recent solution is external water cooling systems. The oil circulates in external coils that pass through water containers. The flow is usually induced by external pumps. One of the advantages is the possibility of having an external oil tank that will store the majority of the oil. In the bearing the only oil present is the necessary for lubrication and for removing the heat from other components. Since the volume of oil in large bearings can reach tens of thousand of litres, the size of the housing will be substantially reduced. In addition, and contrary to the prior solution, if there is a leak, it will be the oil that will infiltrate the coolers and the problem is not as critical since the only purpose of the water is to take energy from the oil.

Although the size of the housing is smaller when using exterior cooling, it is important to assure enough oil inside the housing for proper lubrication in case of failure

Figure 2.15.: Vertical Thrust Bearing Oil Sump and Cooling Coils [4]

of the pumps that inject oil in the bearing. Usually it is specified by contractual obligations that, in case of emergencies such as failure in the cooling system or oil supply to the bearing, the generator has to be able to run for 15 minutes without any damage. This time is enough to stop the machine under safe conditions. During this time the temperatures in the oil should not rise more than 15 ^oC. Otherwise the viscosity of the oil may decrease to values that reduce the film thickness and are out of the safety region [2].

Besides a cooling system, a filtering one is also essential. Its main function is to assure the average size of the particles in the oil injected in the bearing is smaller than the minimum oil film thickness allowed [4]. Generally, the minimum thickness allowed rounds the 20 μm, as a consequence, the filters must retain these particles and larger ones [2].

3. Thrust Bearing Geometry and Operating Conditions

3.1. Introduction

In this chapter, the thrust bearing that will be analysed in this thesis will be presented. Due to confidentiality issues, the exact geometry of the bearing as presented in the technical drawing, will not be shown, instead a simplified geometry that will be used in the calculations will be presented.

The most relevant informations for the analysis of the bearing are the geometry of the pad and the operating conditions of the machine, such as the nominal load and rotational speed, the oil bath temperature and the maximum temperature in the oil flow and the lubricant properties.

3.2. Operating Conditions

The operating conditions of this bearing and the properties of the lubricant are shown in Table 3.1. The mentioned load is a nominal value that includes the weight of the rotating parts and the hydraulic load at the nominal speed of 375 rpm.

The inlet temperature is controlled by a refrigerating system that can be either external or internal. In any case, this temperature is considered constant, only varying with the seasons due to the difference in the temperatures of the refrigerating

Operating Conditions		
Load per pad	712	kN
Rotational Speed	375	rpm
Average Linear Speed	44,67	$m \cdot s^{-1}$
Oil inlet temperature	45	^oC
Oil maximum temperature	63	^oC
Oil Properties		
ISO Grade	46	-
ν at 40 ^oC	46	cSt
ν at 100 ^oC	6,8	cSt
ρ at 15 ^oC	861	$kg \cdot m^{-3}$

Table 3.1.: Bearing operating conditions and oil properties

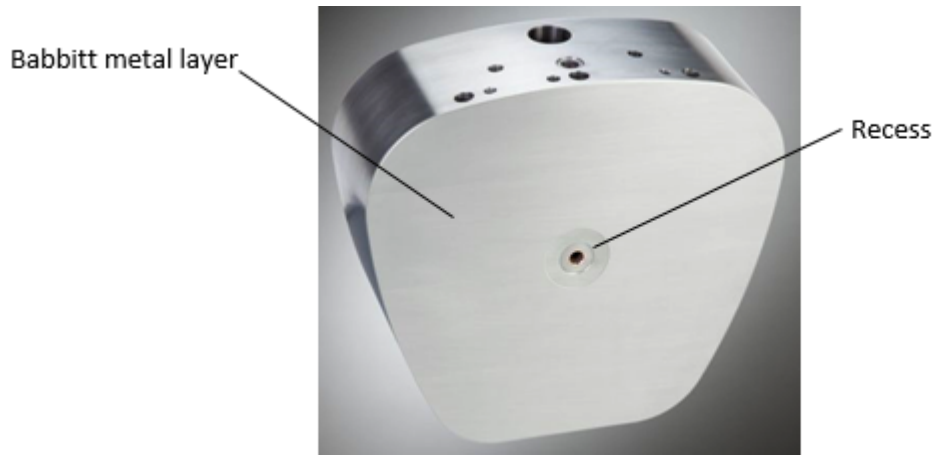

Figure 3.1.: Example of a thrust bearing pad

Geometry		
Inner radius	950	mm
Outer radius	1325	mm
Pad length	496	mm
Number of pads	12	-
Recess diameter	65	mm
Recess height	0,6	mm

Table 3.2.: Bearing Geometry

water. As to the maximum temperature, this value is based on the calculations of the manufacturer of the bearing for the nominal values of load and speed.

3.3. Thrust Bearing Pad Geometry

Figure 3.1 shows a common design for a thrust bearing pad used in bearings for supporting hydro generators. The function of the recess in the middle of the pad, shown in Figure 3.2, is only related to the start up of the machine, a process that will be explained in Chapter 4. Therefore, the recess will not be included in the drawings of the geometry of pad that will be used for further calculations of the hydrodynamic pressure.

Figure 3.3 illustrates the simplified geometry of the thrust bearing pad. Also, table 3.2 presents some additional information such as the number of pads and the size of the recess. As a consequence of being a reversible hydro generator, the pad is symmetrical relatively to a vertical plane that contains the pivot and is perpendicular to the oil flow. On both sides of the pad, it is also possible to observe two ramps that have a relatively small length when compared to the total length of the pad but a significant height. The function of these ramps will be studied further.

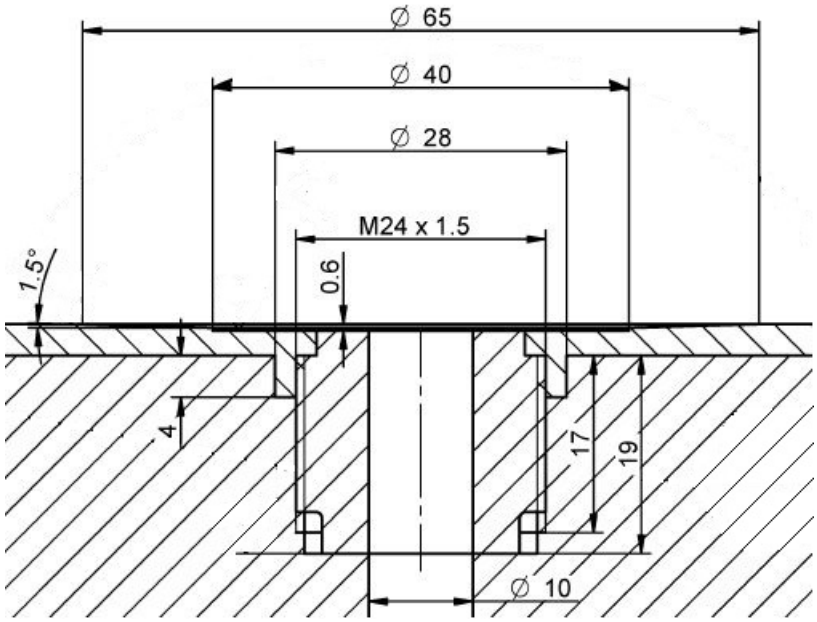

Figure 3.2.: Detail of the recess

3.3.1. Pad surface

The surface of the pad, between the two ramps, is not flat as represented in Figure 3.3. It is a convex surface that reaches a maximum height of 50 μm in the middle of the pad as depicted in Figure 3.4. Although this value may not seem too relevant, it can be more than half of the film height and, therefore, influence the pressure build up.

The main purpose of this convexity may have to do with the fact that this thrust bearing supports a machine whose cycles of operation are highly irregular, since it works both as a turbine and a pump and only works when the network has a need of energy that has to be fulfilled by this power plant. Thus, it is essential to account for the time the machine will be at rest, where contact between the runner and the pad will also have an impact on the dimensioning of these components. A short analysis on the dimension of the area of contact through the Hertz contact theory will allow a better understanding of the objective of this convexity [10].

In Figure 3.5 it is illustrated an example of the type of contact between the pad, surface 1, and the runner, surface 2. The radius of the runner is infinite since this surface is flat. Table 3.3 contains the necessary information to calculate the area of the contact surface when the machine is at rest. Equations 3.1 and 3.2 are used to achieve the values of E^* and R_x.

$$\frac{1}{E^*} = \frac{1-\nu_1^2}{E_1} + \frac{1-\nu_2^2}{E_2} \tag{3.1}$$

$$\frac{1}{R_x} = \frac{1}{2}\left[\frac{1}{R_{x_1}} + \frac{1}{R_{x_2}}\right] \tag{3.2}$$

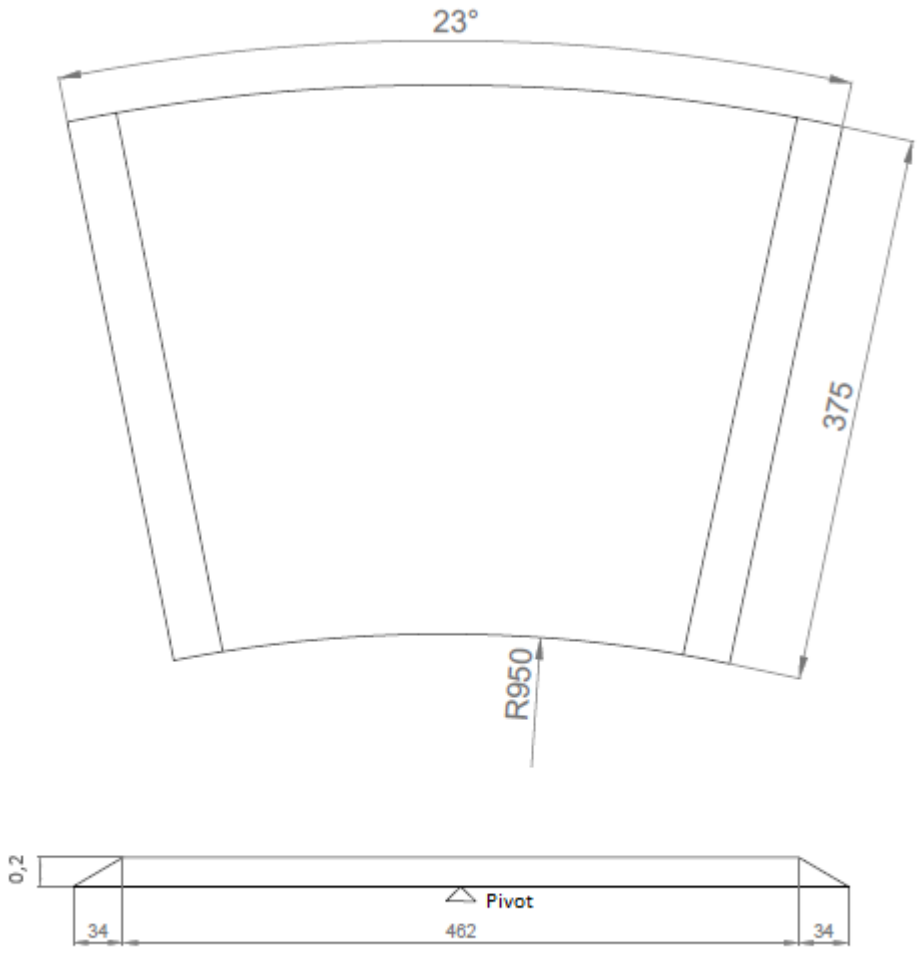

Figure 3.3.: Thrust bearing pad design

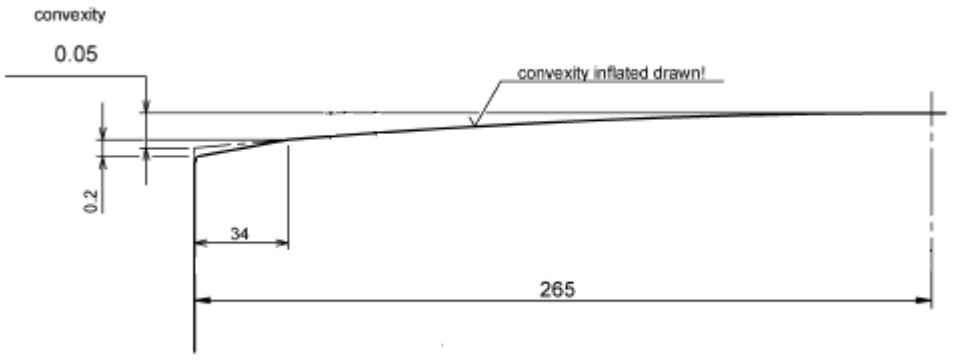

Figure 3.4.: Detail of the surface of the pad represented with inflated convexity

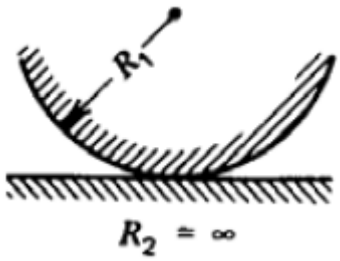

Figure 3.5.: Example of the type of contact between the pad and the runner [10]

Properties		
b	0,375	m
E_{steel}	210	GPa
$E_{babbitt}$	50	GPa
Poisson's ration - ν_1	0,3	-
Poisson's ration - ν_2	0,3	-
R_{x_1}	625	m
R_{x_2}	∞	m
F_n	515,8	kN

Table 3.3.: Data for the Hertz contact theory calculations

$$a = \sqrt{\frac{2\ F_n\ R_x}{\pi\ b\ E^*}} \cong 136\ mm \tag{3.3}$$

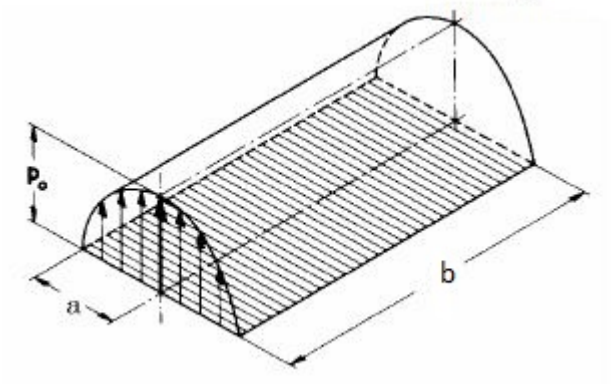

Figure 3.6.: Example of a pressure distribution inside a linear contact [10]

Figure 3.6 illustrates the concept of a half-width of a contact area "a" and a pressure distribution in a linear contact. For this contact, the value of "a" is obtained in

Equation 3.3. Even in the outer radius, where the pad reaches its maximum length, the width of the area of contact, 272 mm, is more than a half of the total length of the flat surface, 462 mm.

Given the substantial area of the contact between the pad and the runner while this last one isn't rotating, it will be assumed that the convexity is present due to the need to support the machine when this one is not working. A flat surface on the pad would, in case of misadjustment, specially in a machine of this size, cause a minor contact area, inducing bigger deformations both on the pad and the runner.

Even though it will introduce inaccuracies in the results, it will be admitted that, under the pressure of the hydrodynamic flow, the surface will deform and the pad will be flat.

4. Hydro Generator Start-Up Procedure: Hydrostatic Lifting

4.1. Introduction

The turbine and generator starting procedure begins with the lifting of the rotating parts of the machine even before they start moving. During this period of time, the thrust bearing works in a hydrostatic lubrication regime by injecting oil in the recess located in the pads.

Regarding the loads these machines have to support and the difficult access for maintenance, it is essential to guarantee the durability and reliability of the bearings, for any failure might cause severe damage to the whole machine. The objective of this procedure is to create an oil film that completely separates the surfaces of the runner and the pad so the machine can start rotating without, theoretically, causing any wear on the materials.

4.2. Hydro Generator Start-up

As a consequence of the condition of a quick response to the power grid, the turbines have to start up as quickly as possible, and have to go through this process several times per day, usually. The oil pumps start working before the rotor starts spinning, injecting the oil in the recesses. The pressure quickly build up and reaches a peak that it is called the "lift pressure" because it is at this point that the runner is lifted and separated from the pads [3].

Right after this peak, the oil flow commences and there is a pressure drop. Only now, when there is an oil film separating the surfaces, the machine starts rotating with the help of an auxiliary system. The high pressure oil injection system is turned off when the speed allows the creation of an oil film in hydrodynamic conditions, which is commonly about 90 % of the nominal speed, in this case, 337,5 rpm. Similarly, when the machine is turned off, the hydrostatic lubrication system is activated in the same conditions, until after immobilization, where enough time is given for the pads and runner to cool down before shutting down the oil pumps. This procedure avoids relative movement between the pads and runner when they are in contact due to different thermal expansion coefficients of the materials.

Recess area	$3,318 \times 10^{-3}$	m^2
Number of pads	12	-
Total area	$39,82 \times 10^{-3}$	m^2
Weight of the rotating parts	6190	kN
Measured lift pressure	325	bar

Table 4.1.: Hydrostatic lift parameters

4.2.1. Analysis of the Lifting Procedure

Table 4.1 presents the lift pressure measured by the pressure gauges placed in oil injection system, the contact area between the oil and the runner and the weight of the rotating parts. In Chapter 3, Figure 3.2, it is possible to observe the recess of the pad, a cylindrical shape with 40 mm diameter surrounded by a conic shape with 65 mm diameter. The contact area presented in this chapter is calculated with the outer diameter of 65 mm. Even though it has to be considered that, when in contact with the runner, the pad surface will deform and part of the conic shape, if not all, might be in contact with the other surface. In case the diameter proves to be bigger than the necessary to lift the machine, the inner diameter of 40 mm will be used.

In order to lift the machine, the load generated by the measured pressure and the contact area of all the twelve pads should be superior to the weight of the machine. Through the definition of pressure, the resulting load is:

$$W = 325 \times 10^5 \times 39,82 \times 10^{-3} = 1294kN \tag{4.1}$$

The load obtained in Equation 4.1 is not enough to lift the machine. Since the weight of the machine is constant and it is known that the 325 bar are enough, the only parameter that must be changed is the contact area. For the same lift pressure and for a 6190 kN, the minimum diameter of the recess to guarantee enough contact area is:

$$D = \sqrt{\frac{\frac{6190 \times 10^3}{12} \times 4}{325 \times 10^5 \times \pi}} = 142,2\ mm \tag{4.2}$$

The value obtained in Equation 4.2 is more than the double of the real diameter of the recess, which means that there must an expansion of the contact area that allows the lifting of the machine. After an interaction with the manufacturer, the following possibility was discussed: The surface of the pad is scraped, which allows the oil to infiltrate the area around the recess, thus creating the conditions for the lifting.

4.3. Conclusions

In this chapter, the start up procedure of the machine was analysed. The results obtained were not the expected, as the area for the hydrostatic lifting as shown in the drawing of the pad proved to be insufficient. The possibility of an expansion of the area through the infiltration of the oil due to the scraped area is not totally confirmed. However, given that the area is the only parameter that can be altered, this possibility was accepted.

5. Analytical Solution for Pressure Distribution in Hydrodynamic Lubrication

5.1. Introduction

In this chapter, an analytical solution of the pressure distribution on the oil film between the runner and a fixed-inclined pad will be presented. This solution will provide the first impression of the aspect of the pressure field.

5.2. Reynolds Equation

In fluid dynamics, the Reynolds number is the ratio between inertial and viscous forces. For fluid film flow, this number is:

$$Re = \frac{U\rho h}{\mu} \tag{5.1}$$

Where U is the average linear speed, ρ is the fluid density, h is the average magnitude of the variable film thickness and μ is the fluid dynamic viscosity. The transition from laminar to turbulent in hydrodynamic lubrication starts at $Re = 1000$ and becomes completely turbulent at $Re = 1600$. [12]

In most bearings, the Reynolds number is sufficiently low to consider there is a laminar flow. The classic hydrodynamic theory is based on the assumption of a linear relation between the fluid shear stress and the strain-rate, in other words, the fluid is considered a Newtonian fluid. Furthermore, under common pressures in hydrodynamic lubrication, the change of volume is negligible, therefore the fluid is considered to be incompressible. [12]

Differential equations are used for theoretical modelling of the flow. These are usually simplified under certain conditions by disregarding therms of a relatively low order of magnitude. An analysis of the order of various terms of an equation, under certain conditions, is required in order to determine the most significant terms which capture the most important effects. A term in an equation can be ignored if it is lower by one or more orders of magnitude in comparison to other terms in the same equation. Dimensionless analysis is a useful and often used tool for determining the

relative orders of magnitude of the terms in an equation [12].

Reynold's equation is used to obtain pressure distributions in the oil film. It is solved through numerical methods, as it is a non-homogeneous partial differential equation of two variables and can not be solved through analytical means [16]. However, if the equation is to be simplified further, by considering the flow isoviscous, only in the x direction and a fixed-inclined pad, the integrated form of Reynolds equation will take this form:

$$\frac{dp}{dx} = 6 \cdot \mu \cdot U \cdot \frac{h - h_m}{h^3} \tag{5.2}$$

Where h_m is the film thickness when $\frac{dp}{dx} = 0$. The oil film thickness h can be written as a function of x [3]:

$$h = h_0 + S_h \left(1 - \frac{x}{L}\right) \tag{5.3}$$

Written this way, the equation was simplified according to the following assumptions [16] [12]:

1. Steady-state condition exists in the oil film
2. The lubricant is incompressible
3. The lubricant is Newtonian
4. Flow is laminar because the Reynolds number is low
5. The fluid adheres to the solid surface at the boundary and there is no fluid slip at the boundary
6. Pressure and shear effects on the viscosity are negligible
7. The variation of the density with the temperature is negligible
8. The velocity component in the z direction is negligible in comparison with the other two components u and v in the x and y directions
9. Velocity gradients along the fluid film in the x and y directions, are small and negligible relative to the velocity gradients across the film
10. The pressure p across the film is constant

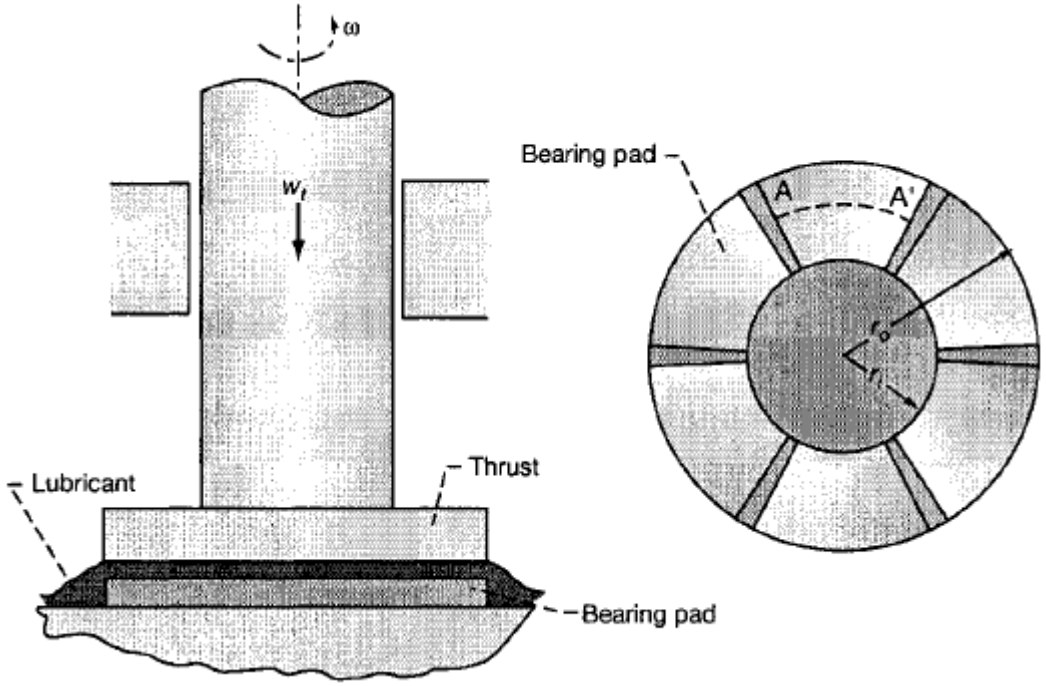

Figure 5.1.: Thrust bearing geometry [3]

Immediate conclusions can be draw when observing Equation 5.2 as it is clear that the pressure gradient along x varies with the oil film thickness and depends on mean tangential velocity, the dynamic viscosity and h_m, that is the film thickness where the pressure gradient is equal to zero. As was mentioned before, and looking to Figure 2.7, the distance h_m that is represented as $J'J$, is where the velocity gradient changes its signal from negative to positive. It is well known that temperature varies along the oil film, resulting in a variation of viscosity. However, due to the significant simplification of the analysis, most of the practical calculations are still based on the assumption of a constant equivalent viscosity that is determined by the average fluid film temperature. The last assumption can be applied in practice because it has already been verified that reasonably accurate results can be obtained for regular hydrodynamic bearings by considering an equivalent viscosity. The average temperature is usually determined by averaging the temperature of the bearing inlet and outlet lubricant [12].

5.3. Thrust Bearing Fixed-Inclined Pad Geometry

Figure 5.1 represents the geometry of a thrust bearing. The section represented by arc AA' is situated in the middle of the pad in the radial direction. As a result of the 1D analysis, the arc AA' represents line along which the values of velocity and pad length will be calculated in this chapter.

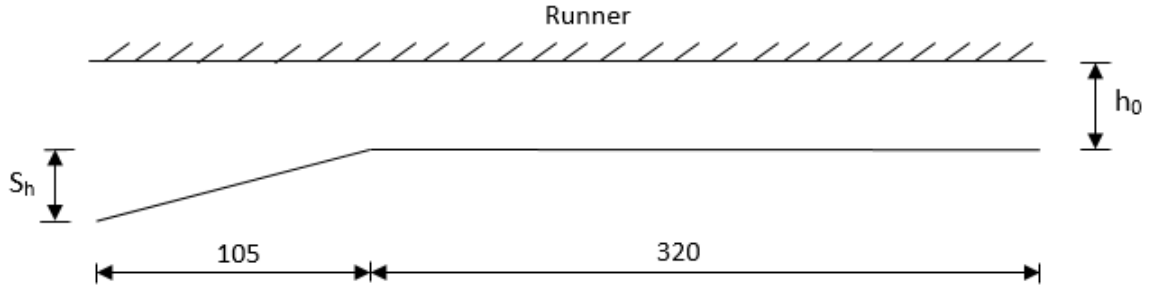

Figure 5.2.: Thrust Pad and Runner Simplified Geometry

A drawing of the pad that will be analysed can be found in Figure 5.2. This simplified geometry will be used in this chapter. The ramp here represented has different dimensions from the pad, as it takes into account the initial ramp and the convexity of the pad. Therefore, the inclination from the ramp and the one from the convexity are considered as one in order to simplify the analysis. The length of this new ramp was calculated through the radius of the convex surface of the pad and its length that becomes flat when under pressure. The ramp of the trailing edge, that would be on the right side, is ignored as it does not contribute to a pressure build up.

The term h_0 represents the oil minimum film thickness. The value that will be considered will be the one provided by the manufacturer in the data sheet of the bearing, since analytical procedures do not permit obtaining it. Therefore, the procedure to find the correct minimum film thickness is to obtain the pressure distribution in the oil film, to calculate the load capacity that derives from this pressure field and compare its value to the load that the bearing has to support. In case the load capacity obtained is not enough, a smaller the value of h_0 must used to repeat the same procedure.

5.3.1. Ramp Analysis

In order to achieve better understanding about the effect of the initial ramp of the pad with a bigger inclination on the leading surface, as illustrated in Figure 5.3, a simple analysis of pressure distribution and normal load is presented. According to Hamrock et al. [3], pressure distribution and normal load component are given by Equations 5.4 and 5.5.

$$p = \frac{6\mu \cdot U \cdot L \cdot X(1-X)}{s_h^2 \left(H_0 + 1 - X\right)^2 \left(1 + 2H_0\right)}, \tag{5.4}$$

$$W = \frac{\mu \cdot U \cdot L^2 \cdot b}{s_h^2} \left[6 \ln \left(\frac{H_0 + 1}{H_0} \right) - \frac{12}{1 + 2H_0} \right] \tag{5.5}$$

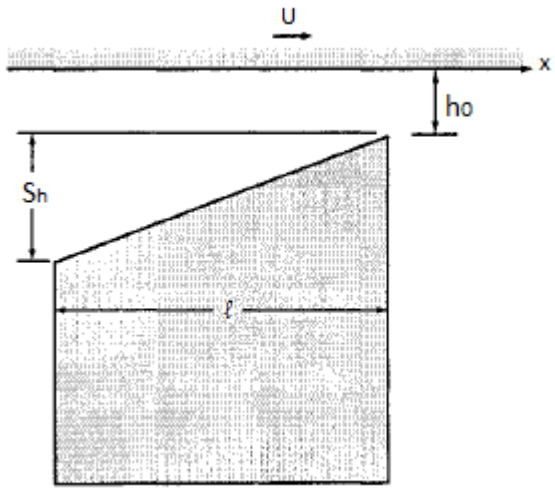

Figure 5.3.: Scheme of the ramp and runner. [3]

Geometry		
h_0	0,090	mm
s_h	0,200	mm
l	34	mm
b	375	mm
Operating Conditions		
U	44,67	$m \cdot s^{-1}$
μ	0,031	$Pa \cdot s$
T_{oil}	45	^oC

Table 5.1.: Ramp geometry and operating conditions

The terms X and H_0 are dimensionless and can be written as:

$$X = \frac{x}{L} \qquad H_0 = \frac{h_0}{S_h} \tag{5.6}$$

The dimensions of the pad and the operating conditions are presented in Table 5.1. The dynamic viscosity, μ was calculated for a temperature of 45 ^oC. The load capacity per pad obtained is:

$$W = 29.75\ kN$$

When analysing the results, it is important to consider the following simplifications:

Geometry		
h_0	0,090	mm
S_h	0,222	mm
L_1	105	mm
L_2	320	mm
b	375	mm

Table 5.2.: Pad geometry

- Only the initial part of the pad is being analysed;
- The pressure on the right side of the ramp being equal to the pressure of the oil bath;
- The heights h_0 and s_h are approximated values.

These have great impact on the output of the prior equations, as it doesn't reflect the reality, but merely gives an idea of what is the role of the initial ramp of the pad. Given that this thrust bearing has twelve segments, the normal load generated is:

$$W_{total} = 357\ kN$$

This value represents far less than the capacity needed to support the machine. Therefore, at first, it is reasonable to assume that this ramp's main function is to create good conditions for the entrance of lubricant in the film and not to generate load.

5.4. Hydrodynamic Pressure Distribution

The dimensions of the pad in Figure 5.2 are presented in Table 5.2. Throughout the process of designing a bearing, the shoulder height, S_h, is a parameter that it is chosen in order to optimize the load carrying capacity. In a pivoted bearing, this value depends on the operating conditions as the pads tilts to find an equilibrium position.

Analytical means do not permit S_h to be a variable, instead a value must be chosen before. Figure 5.4 illustrates the variation of pressure distribution in a fixed-inclined slider bearing with the variation of S_h. According to Hamrock et al. [3], the shoulder height that produces maximum pressure is presented in equation 5.7. Since this value is smaller than the height of the ramp, the analysis will be made with a shoulder height equal to the height of the ramp.

$$S_h = \sqrt{2} \cdot h_0 = 0,127\ mm \tag{5.7}$$

In order to achieve the pressure distribution in the pad, more complicated calculations will be made. Since the height of the oil film, h, does not vary linearly with

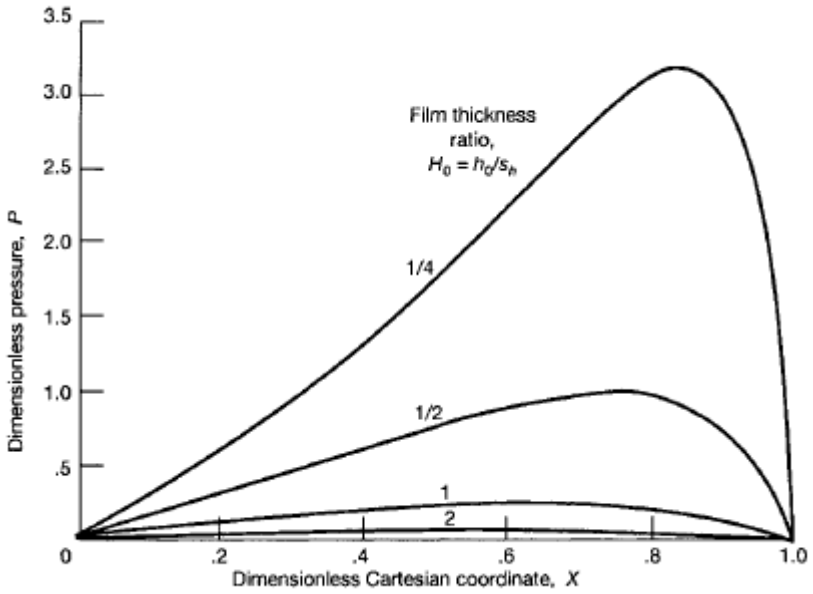

Figure 5.4.: Pressure distribution of fixed-inclined slider bearing [3]

the distance x due to the transition in the end of the ramp, the pad will be divided into two different parts with different inclinations: the ramp, that will be identified with index 1, and the rest of the pad, with index 2.

In this section, it is not possible to use Equation 5.4 because it was simplified with conditions that are not true in this case. Instead Equations 5.8 and 5.9 will be used. Equation 5.8 is integrated from Equation 5.2, considering the substitution presented in Equation 5.3.

Since part of the pad will be parallel to the runner, Equation 5.9 expresses a linear variation of the pressure with the distance. The angle α is the angle that the surface of the ramp makes with an horizontal line. The terms h_m, C, A and B are constants that depend on the conditions that will be imposed. Since there are four constants, two equations must be introduced in order to solve this problem. The four conditions to this problem are:

- p_1 $(h = 290 \times 10^{-6}) = 0$ - The oil pressure is zero before entering the contact.
- p_2 $(h = 90 \times 10^{-6}) = 0$ - The oil pressure is zero in the contact exit.
- The value of pressure in the transition from the ramp to the rest of the pad has to be the same in both equations.
- The oil flow rate, q_1, in the transition of the ramp to the rest of the pad has to be same as q_2.

$$p_1\left(x\right) = -\frac{\mu \cdot U \cdot L}{S_h^2} \cdot \left[\frac{6}{\frac{h_0}{S_h} + 1 - \frac{x}{L}} - \frac{6 \cdot \frac{h_m}{S_h}}{2\left(\frac{h_0}{s_h} + 1 - \frac{x}{L}\right)^2} + C\right] \tag{5.8}$$

$$p_2\left(x\right) = Ax + B \tag{5.9}$$

$$p_1\left(x = 34 \times 10^{-3}\right) = p_2\left(x = 34 \times 10^{-3}\right) \tag{5.10}$$

$$\int_0^b \int_0^h u_1(x = L_1)\, dy\, dz = \int_0^b \int_0^h u_2(x = L_1)\, dy\, dz \tag{5.11}$$

Equations 5.10 and 5.11 express mathematically the last two conditions imposed. Now that there are four unknown variables and four equations, this problem can be solved.

5.4.1. Results

Pressure Distribution

The solution of the system of equations is presented in Equations 5.12 and 5.13. Figure 5.5 shows the representation of these two equations. The blue curve represents the pressure build up in the ramp and the orange the pressure distribution over the rest of the pad. The maximum pressure is 11 Mpa and it is achieved in the transaction between the two lines.

$$p_1\left(x\right) = -1,961 \times 10^6 \cdot \frac{x - 0,1256}{(x - 0,1477)^2} - 11,31 \times 10^6 \tag{5.12}$$

$$p_2\left(x\right) = -34,32 \times 10^6 \cdot x + 14,59 \times 10^6 \tag{5.13}$$

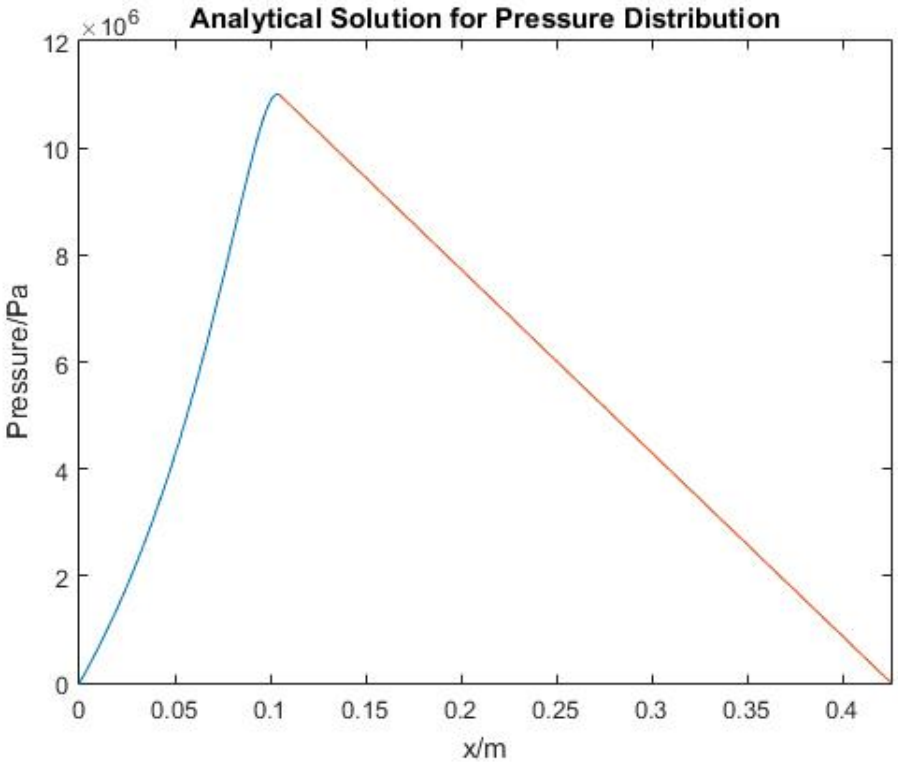

Figure 5.5.: Analytical solution for the pressure distribution

Load Carrying Capacity

The load carrying capacity is obtained by integrating the two functions represented in Equations 5.12 and 5.13, as shown in Equation 5.14.

$$W = \int_0^b \int_0^{L_1} p_1(x)dxdy + \int_0^b \int_{L_1}^{L_2} p_2(x)dxdy \tag{5.14}$$

$$W_{total} = 12 \times W = 10986\ kN \tag{5.15}$$

5.5. Conclusions

This chapter was focused in providing a good perception of the geometry of the thrust bearing pad. The conclusions taken about the ramp and the convexity of the pad allowed a simplification of the geometry. However, assuming the convexity will become flat under pressure is an inaccurate simplification. It would require a much more complicated analysis of both elastic and thermal deformation to really know the shape assumed by the surface. Nevertheless, the assumption made may not be far from reality and provides good results.

Despite being an obsolete method nowadays, the result obtained in this chapter through analytical means is useful to provide an idea of the pressure distribution in

the oil film and to validate further results of a numerical analysis. Moreover, the maximum value of pressure is within the limits of what was expected.

6. Numerical Solution for Pressure Distribution in Hydrodynamic Lubrication

6.1. Introduction

In this chapter a numerical solution for the pressure distribution in the oil film between the runner and the pad will be presented. The solution will be achieved through the Finite Differences Method (FDM). The FDM will be implemented in code using the program MATLAB. A hydrodynamic flow will be studied, disregarding any thermal and elastic deformation of the bearing components.

6.2. Numerical Methods

The differential equations born with the theories of Reynolds and later works rapidly surpassed the capacity of analytical solution. For years, different specialized mathematical functions were develop in an attempt to solve those equations, but they were inefficient and the solutions unsatisfactory. Before numerical methods, there was always a gap between the range of available solutions and what was required in engineering [11].

When, finally, these methods were introduced, there was a radical change in the general understanding and approach to hydrodynamic lubrication. The solutions can now satisfy most of the requirements for prediction of bearing characteristics and the tendency is to improve the quality of these solutions. Problems like how the deformation of the pad affects the load capacity and many others can be now solved with satisfactory predictions [11].

The basic numerical methods used are:

- Finite Difference Method (FDM)
- Finite Element Method (FEM)
- Finite Volume Method (FVM)

These methods divide a continuous area into a finite number of subdivisions, which is called "meshing", and then search and find approximate solutions in each of these

subdivisions. The solution at any point is achieved by interpolation of obtained results. The main differences between these methods are the way of finding the solution, defining the boundary conditions and methods of analysis [17].

6.2.1. Finite Difference Method

According to Hoffman [18], the objective of a FDM for solving a partial differential equation is to transform a calculus problem into an algebra problem by:

1. Discretizing the continuous physical domain into a discrete difference grid
2. Approximating the individual exact partial derivatives in the partial differential equation by algebraic finite differences approximations
3. Substituting the finite differences approximations into the partial differential equation to obtain an algebraic finite difference equation
4. Solving the resulting algebraic finite difference equation

This method is based on approximating a differential quantity by the difference between function values at two or more adjacent nodes. For example, for a random function "M_v", the finite difference approximation to $\frac{\partial M_v}{\partial x*}$ is shown in Figure 6.1, where the subscripts "$i-1$" and "$i+1$" denote the positions immediately behind and in front of the central position i. δx is the step length between nodes [11].

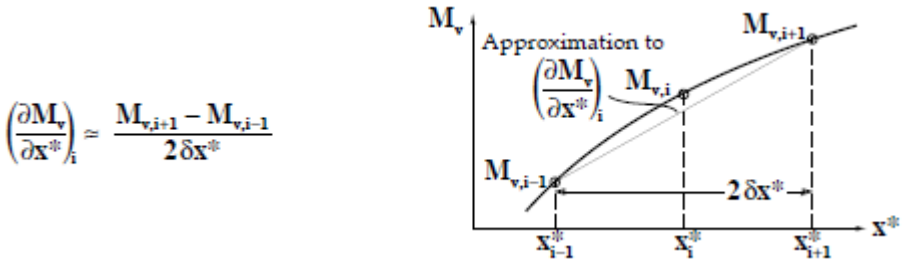

Figure 6.1.: FDM approximation using two adjacent nodes [11]

The finite difference equivalent of $\left(\frac{\partial M_v}{\partial x*} + \frac{\partial M_v}{\partial y*}\right)$ is found by considering the variation of M_v in two axes. A second nodal position variable is introduced along the other axis, the "j" parameter. The expression is exactly the same but the "i" is replaced by "j". Figure 6.2 illustrates a partial grid with five nodes, the central one (i,j) and its adjacent nodes both in the i and j direction [11].

There are several options to take in consideration when developing a finite difference solution to a partial difference equation. Among these, there are the choices of discrete finite difference grid used to discretize the domain of the problem and the finite difference approximations used to represent the individual exact partial

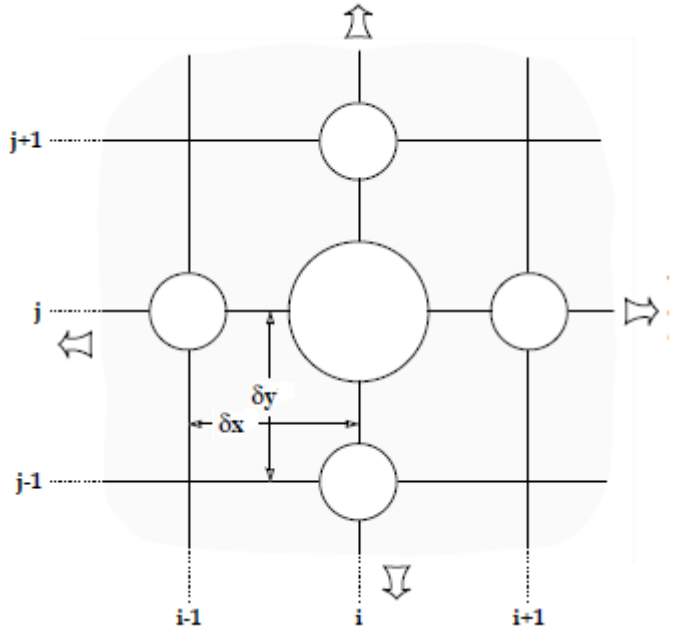

Figure 6.2.: Nodal scheme for numerical analysis of the Reynolds equation [11].

derivatives in the differential equation [18]. In the further sections, the grid and approximation used will be presented.

The main advantages of the FDM are [17]:

- Takes in account the heterogeneity of the material
- Conceptually simple and relatively easy to implement on computer
- Generates a set of equations which are characterized by a unique matrix that allows the use of fast iterative methods for solving this set of equations

And the main disadvantages are [17]:

- Difficulties in taking into account the geometry of irregular shapes
- Can lead to large errors when using a coarse grid
- Despite allowing a local density of mesh nodes, it greatly complicates the implementation of the equations

Despite being less accurate than FEM or FVM, FDM is the simplest of the methods to implement, avoiding the use of computational fluid dynamics (CFD) software, and can be more efficient than the other two when using a uniform structured grid. Nonetheless, the FDM generally produces accurate results when used in fluid dynamics. For these reasons, the method chose to analyse the flow in this thesis was the FDM.

6.3. Reynolds Equation

A basic disadvantage of numerical solutions is that data is only provided for specific values of the variable parameters. For example, a result is obtained for a specific value of friction force for a particular combination of sliding speed, lubricant viscosity, film thickness and bearing dimensions. The process of non-dimensionalization is the replacement of all the real variables in an equation by dimensionless fractions of two or more real parameters. This process extends the generality of a numerical solution. The benefit of non-dimensionalization is that the number of controlling parameters is reduced and a relatively limited data set provides the required information on any bearing [11].

Steady-state condition in the oil film will be considered as the Reynolds equation will be written down in a non dimensional form:

$$2\frac{\partial}{\partial R}\left[\frac{RH^3}{\bar{\mu}}\right]\frac{\partial P}{\partial R}+\frac{2RH^3}{\bar{\mu}}\frac{\partial^2 P}{\partial R^2}+\frac{2}{\beta^2 R}\frac{\partial P}{\partial \bar{\theta}}\frac{\partial}{\partial \theta}\left[\frac{H^3}{\bar{\mu}}\right]+\frac{2}{\beta^2 R}\frac{H^3}{\bar{\mu}}\frac{\partial^2 P}{\partial \bar{\theta}^2}=12R\frac{\partial H}{\partial \theta} \quad (6.1)$$

Where,

$$R=\frac{r}{r_I}\;;\quad \bar{\theta}=\frac{\theta}{\beta}\;;\quad H=\frac{h}{h_0}\;;\quad \bar{\mu}=\frac{\mu}{\mu_0}\;;\quad P=\frac{p\,h_0^2}{6\,\omega\,\mu\,r_I^2}$$

The term β represents the angular extent of the pad. The term $\bar{\mu}$ will be always $\bar{\mu}=1$ given that the flow will be considered isoviscous.

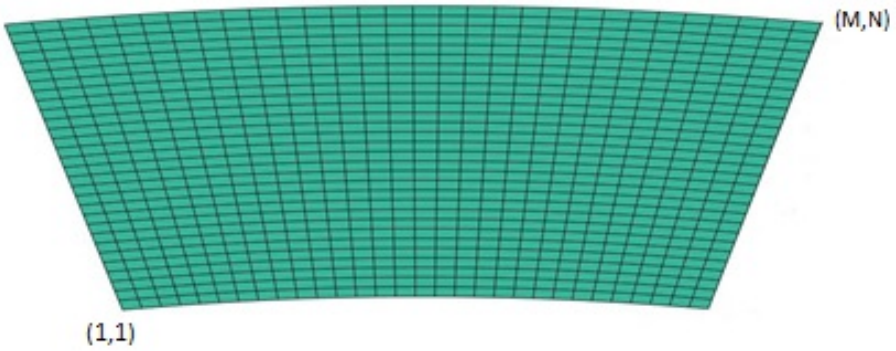

Figure 6.3.: Discretization of the pad with 36x36 nodes

6.4. Computational Procedure

The solution of the Reynolds equation through the finite differences discretization of the thrust pad will be achieved through a total of 961 nodes in form of a grid as shown in Figure 6.3. The approximation to the derivatives present in the differential equation will be done by a truncated Taylor series expansion for three successive nodes. The non dimensional Reynolds equation will now be presented in its finite difference form [16]:

$$\begin{aligned}
&P_{i+1,j}\left[\frac{R_{i,j}\ H_{i,j}^3}{\Delta R^2\ \bar{\mu}_{i,j}}+\frac{R_{i+1,j}\ H_{i+1,j}^3}{\Delta R^2\ \bar{\mu}_{i+1,j}}\right]+P_{i-1,j}\left[\frac{R_{i,j}\ H_{i,j}^3}{\Delta R^2\ \bar{\mu}_{i,j}}+\frac{R_{i-1,j}\ H_{i-1,j}^3}{\Delta R^2\ \bar{\mu}_{i-1,j}}\right]\\
&+P_{i,j+1}\left[\frac{H_{i,j}^3}{R_{i,j}\ \bar{\mu}_{i,j}\ \beta^2\ \Delta\bar{\theta}^2}+\frac{H_{i,j+1}^3}{R_{i,j}\ \bar{\mu}_{i,j+1}\ \beta^2\ \Delta\bar{\theta}^2}\right]\\
&+P_{i,j-1}\left[\frac{H_{i,j}^3}{R_{i,j}\ \bar{\mu}_{i,j}\ \beta^2\ \Delta\bar{\theta}^2}+\frac{H_{i,j-1}^3}{R_{i,j}\ \bar{\mu}_{i,j-1}\ \beta^2\ \Delta\bar{\theta}^2}\right]\\
&+P_{i,j}\Big[-2\cdot\frac{R_{i,j}\ H_{i,j}^3}{\Delta R^2\ \bar{\mu}_{i,j}}-\frac{R_{i+1,j}\ H_{i+1,j}^3}{\Delta R^2\ \bar{\mu}_{i+1,j}}-\frac{R_{i-1,j}\ H_{i-1,j}^3}{\Delta R^2\ \bar{\mu}_{i-1,j}}\\
&-2\cdot\frac{H_{i,j}^3}{R_{i,j}\ \bar{\mu}_{i,j}\ \beta^2\ \Delta\bar{\theta}^2}-\frac{H_{i,j+1}^3}{R_{i,j}\ \bar{\mu}_{i,j+1}\ \beta^2\ \Delta\bar{\theta}^2}-\frac{H_{i,j-1}^3}{R_{i,j}\ \bar{\mu}_{i,j-1}\ \beta^2\ \Delta\bar{\theta}^2}\Big]\\
&=\frac{6\ R_{i,j}}{\Delta\theta}\left[H_{i,j+1}-H_{i,j-1}\right]
\end{aligned}\tag{6.2}$$

Equation 6.2 is now a set of algebraic equations, which will be transformed in a matrix and solved simultaneously by subroutines, producing the values of non-dimensional pressure in each node. But first, the equation will be manipulated and presented in a more simple form. Since the objective is to know the pressure field, $P_{i,j}$ will be isolated in one side. Also the matrix $\bar{\mu}_{i,j}$ will de removed, for the same reason mentioned before, which will also facilitate the manipulation of the equation:

$$P_{i,j}=\frac{1}{A}\left[B\cdot P_{i+1,j}+C\cdot P_{i-1,j}+D\cdot P_{i,j+1}+E\cdot P_{i,j-1}-F\right]\tag{6.3}$$

Where,

$$A=\frac{2R_{i,j}\ H_{i,j}^3+R_{i+1,j}\ H_{i+1,j}^3+R_{i-1,j}\ H_{i-1,j}^3}{\Delta R^2}+\frac{2H_{i,j}^3+H_{i,j+1}^3+H_{i,j-1}^3}{R_{i,j}\ \beta^2\ \Delta\bar{\theta}^2}$$

$$B=\frac{R_{i,j}\ H_{i,j}^3+R_{i+1,j}\ H_{i+1,j}^3}{\Delta R^2}$$

$$C = \frac{R_{i,j}\ H_{i,j}^3 + R_{i-1,j}\ H_{i-1,j}^3}{\Delta R^2}$$

$$D = \frac{H_{i,j}^3 + H_{i,j+1}^3}{R_{i,j}\ \beta^2\ \Delta\bar{\theta}^2}$$

$$E = \frac{H_{i,j}^3 + H_{i,j-1}^3}{R_{i,j}\ \beta^2\ \Delta\bar{\theta}^2}$$

$$F = \frac{6\ R_{i,j}}{\Delta\theta}\left[H_{i,j+1} - H_{i,j-1}\right]$$

The number of nodes 961, where $M = N = 31$, was chosen based on the conclusions drawn by Najar and Harmain [19], where several grid sizes were studied, from 12×12 until 96×96, and concluded that grid sizes bigger than 24×24 do not show further significant improvement, although the results will vary. Furthermore, a tight tolerance value is was chosen to ensure the numerical derivative calculated by the algorithm is precise:

$$\sum_{i=2}^{M-1}\sum_{j=2}^{N-1}\frac{|P_{i,j}^{new} - P_{i,j}^{old}|}{|P_{i,j}^{new}|} \leq \epsilon_r \tag{6.4}$$

Where ϵ_r is the tolerance limit. The calculations of the dimensional form of the Reynolds equation and the load capacity generated are shown in Equations 6.5 and 6.6. The value chosen was 0.1%. The MATLAB code used is displayed in Appendices A.

$$p(i,j) = \frac{6\ P(i,j)\ \omega\ \mu\ r_1^2}{h_0^2} \tag{6.5}$$

$$W = \sum_{1}^{36}\sum_{1}^{36} p(i,j)\ r(i,j)\ d\theta\ dr \tag{6.6}$$

6.5. Results

The results obtained in FDM code used will be presented in the next sections, where different cases will be studied. The minimum film height and the tilting of the pad will be varied and the resulting load capacity compared with the nominal load of the machine.

6.5.1. Fixed-Inclined Pad

For the exact same configuration of the pad presented in Chapter 5, Figures 6.4 and 6.5 represent the film height distribution and the pressure distribution on the pad. The two breaks that can be observed in the first image, on the left, have to do

with the way the surface was discretized. The matrix that represents the film height is composed by two smaller ones, one that represents the film height in the ramp and another that represents the rest of the surface. The problem is when advancing to the next row of nodes, for two times, two consecutive nodes in the same column were placed in a different matrix, one in the ramp and the other in the other surface, causing this effect. With a bigger number of nodes these breaks would disappear, however a bigger number nodes implies an accumulation of truncation errors, the disadvantage of finer grids.

Observing the pressure distribution, the maximum pressure obtained is too high, reaching the 28,5 MPa and a load capacity of 1200 kN per pad, which is almost the double of the load that each pad has to support. Therefore, the minimum film height considered, 90 μm is too small and generates more load capacity than the one needed. In order to descend this value to the correct one, the film height would have to be increased.

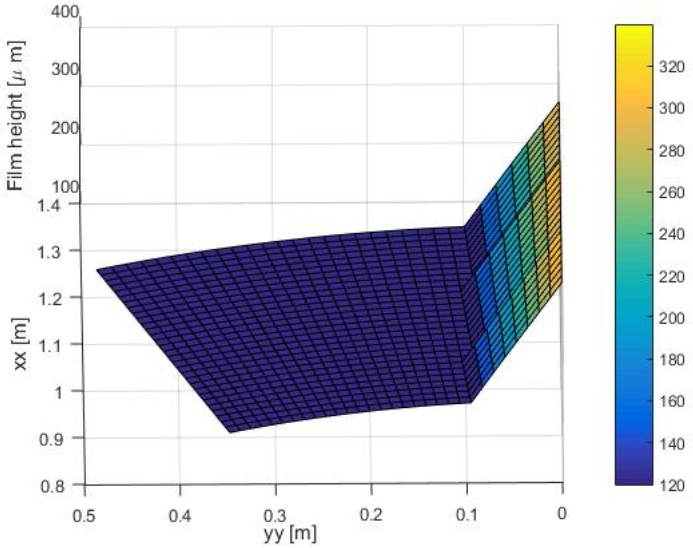

Figure 6.4.: Film height over the pad

6.5.2. Optimum Minimum Film Thickness and Tilting

Considering now the pad is allowed to tilt, Figure 6.6 illustrates the oil film height distribution along the pad. The dynamic viscosity considered in this calculation is $\mu = 0,015\ Pa \cdot s$, calculated for $T = 63\ ^oC$, the maximum temperature inside the contact, which is a conservative calculation given that the load capacity will be less in these conditions. It is possible to distinguish two different inclinations once more, the ramp and the tilting of the pad. The values were achieved by scanning the values of minimum film height and, for each value of the height, scanning the inclination of the pad to find the maximum load capacity. Finally, the optimum result achieved was 154 μm for the minimum film thickness and 147 μm for the tilting, which results

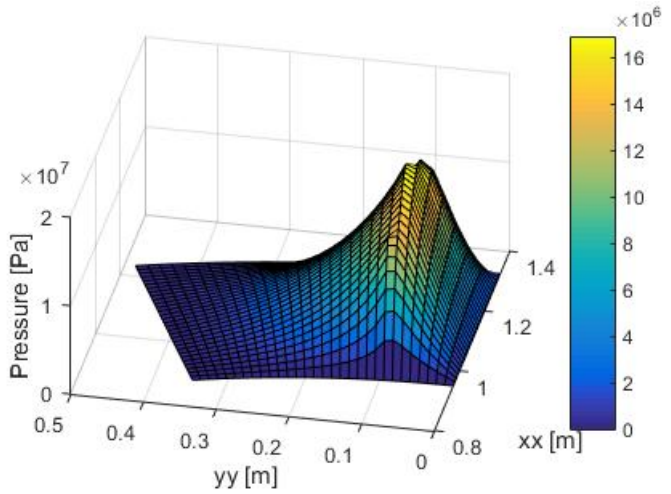

Figure 6.5.: Pressure distribution in the oil film

in a total shoulder height of 347 μm. Figures 6.7 and 6.8 show the pressure wave over the pad. This distribution provides the necessary load capacity to support the machine with a maximum pressure of 10 MPa. The average pressure over the pad is 3.9 MPa. The load capacity generated equals the nominal load of the machine, $W = 8548\ kN$.

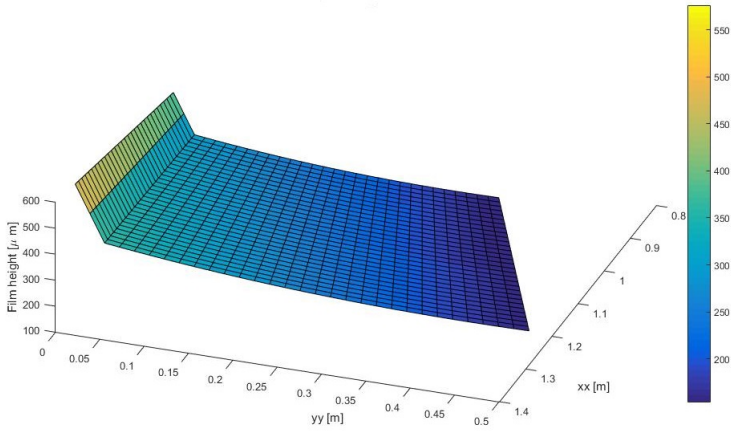

Figure 6.6.: Film height over the pad

6.6. Conclusions

This chapter was focused on a numerical solution of the hydrodynamic flow inside a thrust bearing through FDM. Two different geometries were analysed, the fixed-inclined pad that had already been object of study in Chapter 5 and a new geometry that considers the tilting of the pad. The grid used was chosen based in the experience of other authors who studied the effect of the number of nodes in the results. It should not be too coarse to analyse too few points and not providing a correct

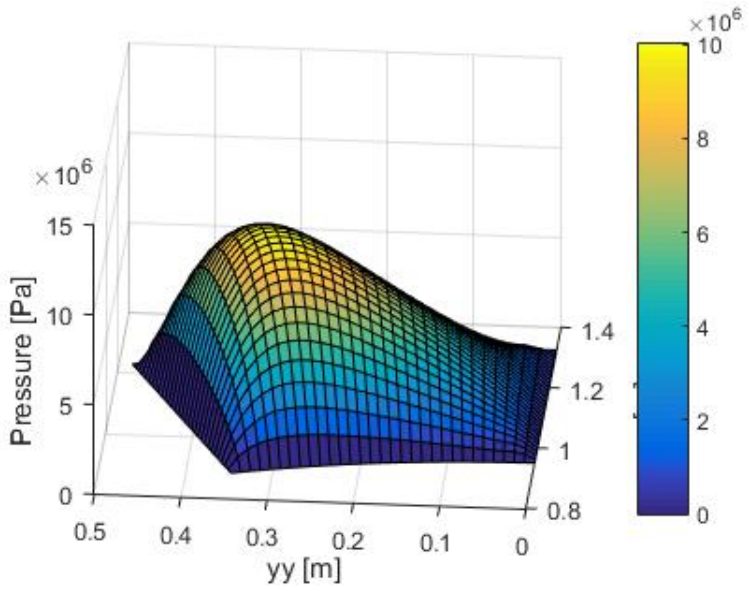

Figure 6.7.: Pressure distribution in the oil film

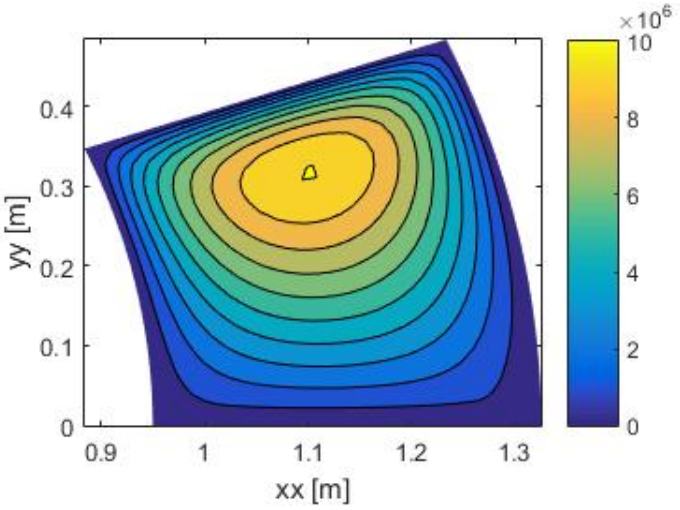

Figure 6.8.: Pressure distribution in the oil film

distribution and not too fine that would accumulate truncation errors and spend unnecessary computational time.

The results obtained with the first solution present a bad distribution of pressure, resulting in a higher value for the maximum pressure and in a lower load capacity. However, a comparison can be made between both configurations in order to understand the importance and effects of the pivot. The second solution produces better results, as it achieves higher load capacity with a bigger minimum film height and a lower maximum pressure. Also distribution obtained is similar to solutions presented in other articles such as [19] and [20].

Nevertheless, the results differ from the ones provided in the data sheet of the bearing. Instead of a minimum oil film thickness of 90 μm, the results obtained were for 154 μm of minimum film thickness. Also the average working pressure is 3,9 MPa instead of 3,2 MPa as indicated by the manufacturer. These differences are a consequence of a simplified geometry that neglects the thermal and elastic deformation and for considering an isothermal and isoviscous flow. Also, the tilting of the pad should be calculated through a momentum equilibrium on the pivot.

7. Conclusions and Future Work Perspectives

The main objective of this thesis was to calculate the operating conditions of a hydrodynamic thrust bearing assembled in a hydroelectric generator and compare these results to the ones provided by the manufacturer. In order to establish this comparison, accurate performance parameters as minimum oil film thickness, pressure distribution and tilting angle had to be determined.

The lubrication theory of Reynolds was used and its equations adapted, in a bi-dimensional form, to a hydrodynamic thrust bearing pad. Analytical means to solve the equation were used and the pressure distribution on the circumferential direction along the mean radius of the bearing was presented. The finite difference form of the Reynolds equation was solved by a FDM algorithm using three consecutive nodes for the approximation of the derivatives and the resulting pressure field and optimum tilting and minimum oil film thickness calculated.

The results obtained differed from the parameters provided in the data sheet of the bearing. All the assumptions made about some of the characteristics of the bearing, both in the geometry and operating conditions, led to less accurate results. As a consequence, a larger minimum thickness oil film was presented as the one necessary to support the load resulting from the weight of the machine and the hydraulic load.

7.1. Future Work

For future work related to this theme it would be interesting to further develop the FDM algorithm for the numerical analysis. There are many ways in which it can be improved, starting by introducing the Energy equation so that the oil temperature field over the bearing can be calculated. This would allow the study of the variation of viscosity along the film and, thus, permit a more accurate analysis. Regarding the tilting movement of the pad, a momentum equilibrium analysis around the pivot would also improve the algorithm.

Besides the hydrodynamic analysis, including the thermal and elastic deformation of the surfaces of the pad and runner would further increase the accuracy of the results. This analysis is called an elasto-thermo-hydrodynamic analysis (TEHD) and it is the state of the art method to perform analysis on these bearings. Finally, it would be also interesting to use a computational fluid dynamics software such as ANSYS or, instead of the FDM use the FEM.

Bibliography

[1] ASME, "The kingsbury bearing at holtwood," *http://www.kingsbury.com/file_library.shtml*, 2016.

[2] P. Pajączkowski, *Simulation of transient states in large hydrodynamic thrust bearings*. Phd thesis, 2010.

[3] B. J. Hamrock, S. R. Schmid, and B. O. Jacobson, *Fundamentals of Fluid Film Lubrification*, vol. 2nd ed. New York: McGraw Hill, 1994.

[4] I. Kingsbury, "A general guide to the principles, operation and troubleshooting of: Hydrodynamic bearings," 2016.

[5] R. W. Bruce, *Handbook of Lubrication and Tribology, Volume II: Theory and Design*, vol. 2. CRC press, 2012.

[6] K. Tschauder and J. Leather, "Nrel tribology seminar fundamentals of lubrication gear oil formulation," 2011.

[7] A. Leopard, "Tilting pad bearings-limits of operation," *Lubrication Engineering*, vol. 32, no. 12, pp. 637–644, 1976.

[8] D. R. Garner and A. Leopard, "Temperature measurements in fluid film bearings," in *Proceedings of the 13th Turbomachinery Symposium, College Station, Texas*, pp. 133–137, 1985.

[9] S. Glavatskih, "A method of temperature monitoring in fluid film bearings," *Tribology International*, vol. 37, no. 2, pp. 143 – 148, 2004. Austrib 2002.

[10] J. Seabra, *Mecânica do Contacto Hertziano*. SMAp, DEMEGI, FEUP, 2003.

[11] G. W. Stachowiak and A. W. Batchelor, *Engineering Tribology*. Butterworth-Heinemann, 1993.

[12] A. Harnoy, *Bearing design in machinery: engineering tribology and lubrication*. CRC press, 2002.

[13] L. Drabowski and M. Wasilczuk, "Evaluation of water turbine hydrodynamic thrust bearing performance on the basis of thermoelastohydrodynamic calculations and operational data," 2004.

[14] T. Mang and W. Dresel, *Lubricants and Lubrication*. John Wiley & Sons, 2007.

[15] L. A. d. A. Ferreira, *Tribologia: Notas de Curso*. Porto: Publindústria, 1998.

[16] D. Srikanth, K. K. Chaturvedi, and A. C. K. Reddy, "Determination of a large tilting pad thrust bearing angular stiffness," *Tribology International*, vol. 47, pp. 69 – 76, 2012.

[17] W. Graboń and J. Smykla, "Computer program for symulation of pressure distribution in the hydrodynamic radial bearing," *Artificial Intelligence Driven Solutions to Business and Engineering Problems*, p. 176, 2012.

[18] J. D. Hoffman, *Numerical Methods for Engineers and Scientists*. Marcel Dekker, 2nd ed., rev. and expanded ed., 2001.

[19] F. A. Najar and G. A. Harmain, "Numerical investigation of pressure profile in hydrodynamic lubrication thrust bearing," *International Scholarly Research Notices*, vol. 2014, p. 8, 2014.

[20] D. Srikanth, K. Chaturvedi, and A. C. K. Reddy, "Modelling of large tilting pad thrust bearing stiffness and damping coefficients," *Tribology in industry*, vol. 31, no. 3&4, 2009.

Appendices

A. MATLAB Code

```
clear; clc;
%% input
N=31;
M=N;
Nrad=375*pi()/30; %rad/s

RR1=1.900/2; % raio interior em m
RR2=1.900/2+0.500-0.125; % raio exterior em m
R1=1; %raio interior adimensional
R2=RR2/RR1; %raio exterior adimensional

Thetat=21.5; %degrees
Thetat=Thetat*pi()/180; %rad

dt=1/(N-1); %incremento em theta adimensional
dT=dt*Thetat; %incremento em theta

dr=(R2-R1)/(M-1); %incremento em R
dR=dr*RR1;
H0=154.5e-6; %espessura minima de filme m
%Hs=0;
Hs=0.95*H0; %H1-H0 m

mu=1; % viscosidade adimensional
mur=15.4e-3; %viscosidade dinamica Pa*s

ITER=1000; % n maximo de iteracoes


%inclinacao do patim
%Convergente/chanfro
hc=0.2e-3;% altura do chanfro m
lc=34e-3; %largura do chanfro m
beta=atan(hc/lc); %inclinacao do chanfro

alfa=atan(Hs/(RR1*Thetat-lc)); %inclinacao da parte plana do patim definida a partir
                                %de Hs



%% iniciacao das matrizes de raio, angulo, altura de filme e pressao
for i=1:N;
    for j=1:M;
        R(i,j)=R1+dr*(i-1);
        t(i,j)=1-dt*(j-1);
```

```
        %h(i,j)=1+Hs/H0*(1-t(i,j)); % definicao de h para versao de patim plano

        %_________ definicao de h para versao de patim com chanfro
        gama(i)=atan(lc/(R(i,1)*RR1)); %angulo do chanfro em funcao do raio
        gamaa(i)=gama(i)/Thetat; %angulo chanfro adimensional
        if t(i,j)>gamaa(i)
            temp=j;
            h(i,j)=1+RR1*R(i,j)*((j-1)*dT)*tan(alfa)/H0;
        else
            h(i,j)=1+RR1*R(i,temp)*((temp)*dT)*tan(alfa)/H0+RR1*R(i,j)
            *((j-1)*dT-temp*dT)*tan(alfa+beta)/H0;
        end
        %_________

        p(i,j)=0.0;
        P(i,j)=0.0;

        x(i,j)=RR1*R(i,j)*cos(Thetat*t(i,j));
        y(i,j)=RR1*R(i,j)*sin(Thetat*t(i,j));

    end
end
%surf(x,y,h); hold; surf(x,y,h2)
cubh=h.^3;


%% Diferencas finitas
sum(1)=0.0;
for K=1:ITER;
    sumij=0.0;
    for i=2:N-1;
        for j=2:M-1;
            A=(2*R(i,j)*cubh(i,j)+R(i+1,j)*cubh(i+1,j)+R(i-1,j)*cubh(i-1,j))/(dr^2*mu)
            +(2*cubh(i,j)+cubh(i,j+1)+cubh(i,j-1))/(R(i,j)*mu*Thetat^2*dt^2);
            B=(R(i,j)*cubh(i,j)+R(i+1,j)*cubh(i+1,j))/(dr^2*mu);
            C=(R(i,j)*cubh(i,j)+R(i-1,j)*cubh(i-1,j))/(dr^2*mu);
            D=(cubh(i,j)+cubh(i,j+1))/(R(i,j)*mu*Thetat^2*dt^2);
            E=(cubh(i,j)+cubh(i,j-1))/(R(i,j)*mu*Thetat^2*dt^2);
            F=6*R(i,j)*(h(i,j+1)-h(i,j-1))/dT;
            p(i,j)=(1/A)*(B*p(i+1,j)+C*p(i-1,j)+D*p(i,j+1)+E*p(i,j-1)-F);
            sumij=sumij+p(i,j);
            P(i,j)=(p(i,j)*6*Nrad*mur*RR1^2)/H0^2;
        end
    end
    sum(K+1)=sumij;
    percentage=abs(sum(K+1)-sum(K))/abs(sum(K+1));
    if percentage < 0.001;
    break
    end
end

p=-p;
P=-P;
K %numero de iteracoes

%% Calculo da capacidade de carga
```

```
W=0;
for i=1:N
    for j=1:M
        W=W+P(i,j)*R(i,j)*dT*dR;
    end
end
W
WT=W/1000;
Pmax=max(max(P))/1e6
```